NASA CONTRACTOR REPORT

NASA CR-2347

NASA CR-2347

SPOKED WHEELS TO DEPLOY LARGE SURFACES IN SPACE - WEIGHT ESTIMATES FOR SOLAR ARRAYS

R. F. Crawford, J. M. Hedgepeth, and P. R. Preiswerk

Prepared by
ASTRO RESEARCH CORPORATION
Santa Barbara, Calif. 93103
for Ames Research Center

NATIONAL AERONAUTICS AND SPACE ADMINISTRATION • WASHINGTON, D. C. • JANUARY 1975

1. Report No.	2. Government Accession No.	3. Recipient's Catalog No.
NASA CR-2347		

4. Title and Subtitle	5. Report Date
SPOKED WHEELS TO DEPLOY LARGE SURFACES IN SPACE - WEIGHT ESTIMATES FOR SOLAR ARRAYS	January 1975
	6. Performing Organization Code
7. Author(s)	8. Performing Organization Report No.
R. F. Crawford, J. M. Hedgepeth, and P. R. Preiswerk	ARC-R-1004
	10. Work Unit No.
9. Performing Organization Name and Address	11. Contract or Grant No.
Astro Research Corporation Santa Barbara, CA 93103	NAS2-6731
	13. Type of Report and Period Covered
12. Sponsoring Agency Name and Address	Contractor Final Report
National Aeronautics and Space Administration Washington, D.C. 20546	14. Sponsoring Agency Code

15. Supplementary Notes

16. Abstract

A study of concepts to deploy large surfaces in space to provide support structures for solar arrays and other functions.

17. Key Words (Suggested by Author(s))	18. Distribution Statement
Space structures, deployable structures, solar arrays, spoked wheels.	Unlimited

19. Security Classif. (of this report)	20. Security Classif. (of this page)	21. No. of Pages	22. Price*
Unclassified	Unclassified	60	$4.25

*For sale by the National Technical Information Service, Springfield, Virginia 22151

CONTENTS

ILLUSTRATIONS

ILLUSTRATIONS (cont'd)

INTRODUCTION AND SUMMARY

Trends for projected space experiments and applications of space technology indicate future demands for energy collectors and transmitters, reflectors, communication antennas, and Earth-resource sensors of increasingly large surface areas. However, means for efficiently packaging, deploying, and structurally supporting such surfaces do not appear to exist, especially when the areas must be very large.

Solar-cell arrays constitute a current application of large-area space structures. Extensible booms have been used to deploy and support solar-cell arrays of varying areas. Hughes Aircraft Company, Reference 1; Jet Propulsion Laboratory (JPL), Reference 2; and Lockheed Missiles and Space Company, Incorporated (LMSC), Reference 3, have studied and built solar-cell array systems in which, generally, one or two booms are used to deploy and tension a blanket with attached cells and bussing. But Reference 4 and routine scaling analyses show that a scale-up of such boom concepts for very large solar-cell blankets would result in a substantial increase in the structural weight fractions of the systems. Besides this scaling problem, these boom-deployed, planar surfaces are not useful for collecting and concentrating radiant energy, or for accomplishing the other possible tasks for which large areas are required. This type of planar arrangement is not structurally deep. Accordingly, it is not well suited for minimizing thermal distortions or otherwise maintaining dimensional stability, as might be required by a large antenna.

For these reasons, another structural concept is examined herein. It is that of a segmented and hinged rim, supported by spokes joined to a common hub as pictured in Figure 1. It is clearly based on the same concept as a spoked wheel. However, Figure 1 also indicates that, by segmenting and hinging the rim, this structure can be compactly packaged and deployed.

This deployable structure is described and some of its uses are discussed in the present report. In addition, a preliminary, parametric analysis is performed to estimate weight fractions of the structure when it is designed for deploying and supporting solar-cell arrays of large areas. The design requirement that dominates the analysis is that the blanket must be sufficiently tensioned to provide a specified vibrational frequency. The structural components are designed to withstand their reactions

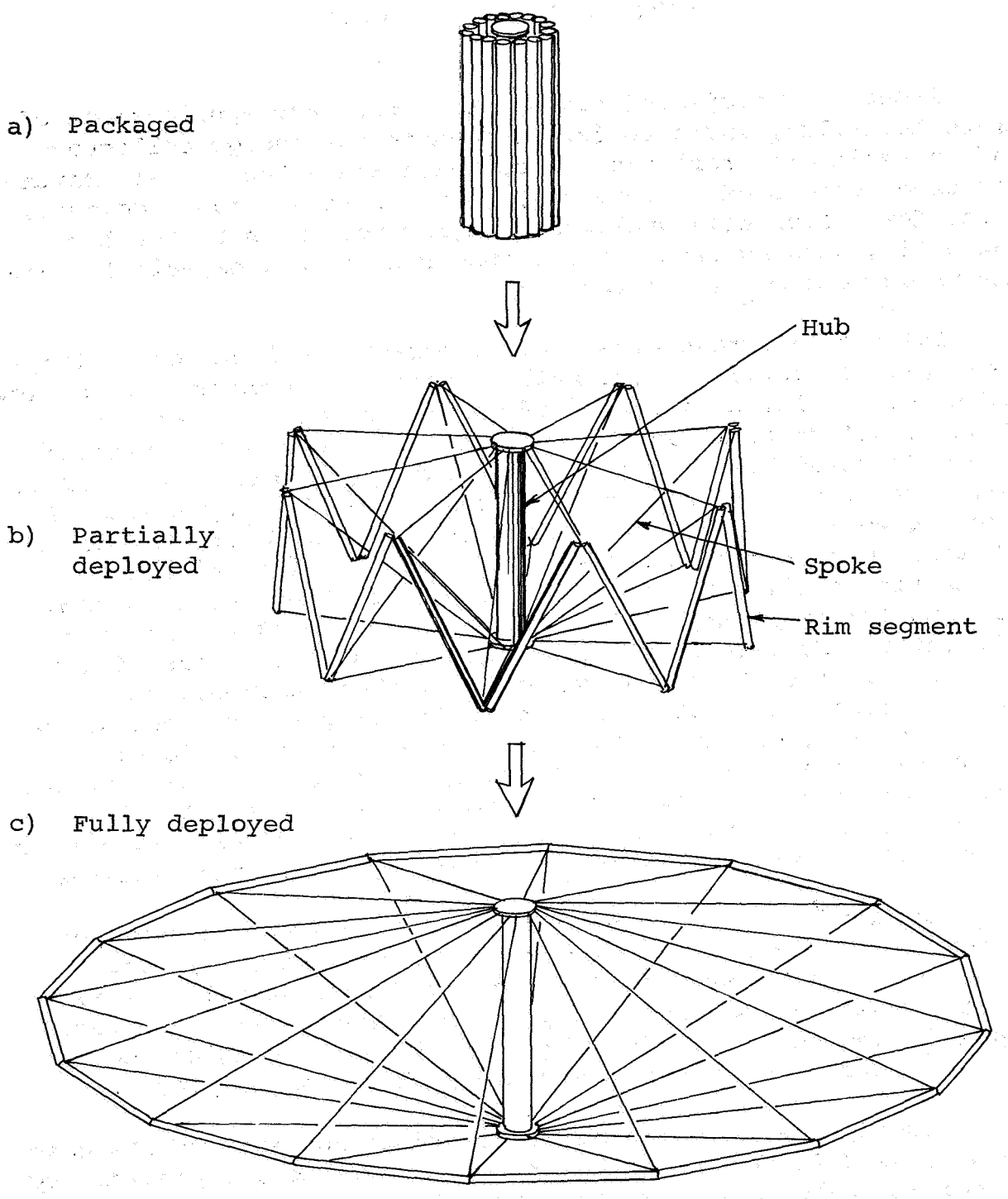

Figure 1. Segmented-Rim Structure for Deploying Space Equipment

to that tension. Assumptions are made in the analysis which enable rapid estimation of weight. The results are believed to be accurate enough to demonstrate trends; of course, detailed design may introduce moderate changes in weights.

The analytical results show that structural weight fractions for the deployable-rim concept will be significantly smaller than those for the existing boom-deployed arrays. As the areas are increased, while the required vibrational frequency is held constant, the weight fractions increase substantially. A scaling relationship between control frequencies (hence vibrational frequencies) and blanket area is suggested for this application, where the function of the control system is to maintain the angular orientation of the blanket to the sun within certain prescribed limits. When that relationship is observed, the increase in structural weight fraction with area is not as great as when the frequency is held constant. These results are presented graphically.

The results show the deployable rim to be a feasible and efficient means for deploying solar arrays of large areas. These potentials should be more fully examined, and similar investigations should be made of the spoked-wheel capability for deploying other types of large surfaces.

DESCRIPTION OF THE DEPLOYABLE SPOKED WHEEL

Design aspects of this foldable structure, independent of utilization, are described below. Subsequently, a few applications are discussed, with emphasis on the deployment of solar-cell arrays.

Design Aspects

Figure 1 depicts the general concept of this rigid, nonspinning deployable structure. Its rim is foldable because of the manner in which it is segmented and hinged. Two sets of spokes structurally stabilize the rim, one set extending to each end of the common hub. The hub axis is perpendicular to the plane of the deployed rim. Thus, the concept utilizes the same structural principles as the ordinary spoked wheel, except that, in this case, the rim is foldable.

The rim must consist of an even number (four or more) of equal-length, hinged segments, if it is to fold as shown in Figure 1. Two methods of hinging were conceived that permit folding of the rim. One method is shown in Figure 2, where each joint between the rim segments is seen to involve two hinges and an intermediate block. The two hinges join ends of adjacent rim segments to the block. The two hinges on a block have axes that lie in the same plane but are not parallel. As shown in Figure 2, each hinge axis must be perpendicular to the hub axis, as well as to the axis of the rim segment to which it is attached. So hinged, the rim deploys freely so long as the midlengths of all rim segments move synchronously in a radial direction from the hub axis. Accordingly, each segment of the rim deploys by rotating about its own midlength while translating radially outward.

The second method of hinging uses only one hinge in the joint between adjacent segments, but the segments undergo rotations about their axes as they deploy. That method and its analytical derivation are described in the attached Appendix A.

To deploy either of these two types of rims, it is necessary to apply torques at the hinges to cause synchronized spreading of all joints. One method of applying the torques can be to install preloaded torsion springs at the hinges and to meter

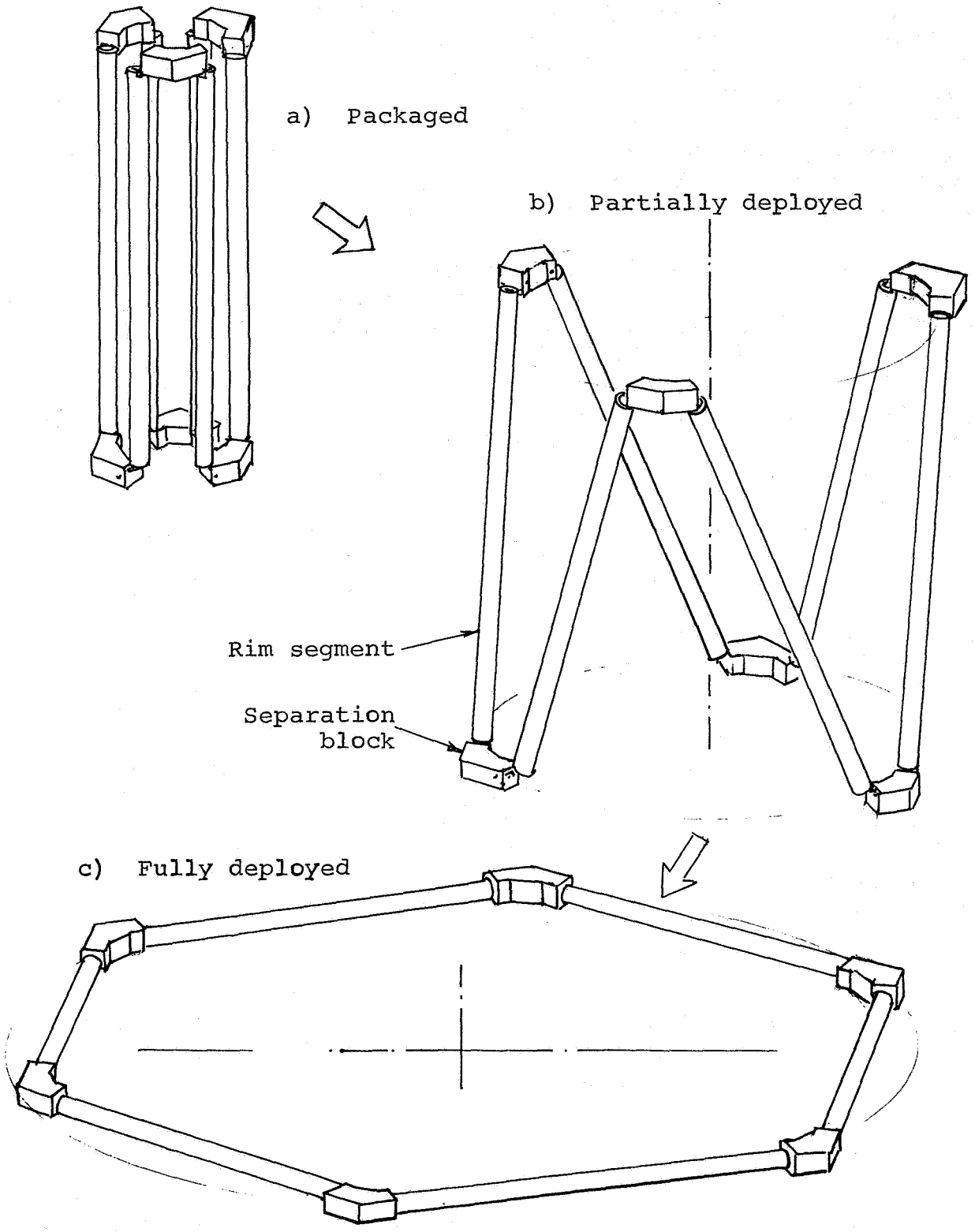

Figure 2. Two-Hinge Method for Deploying Rim

the spokes outward to ensure synchronized spreading of all the hinges. This method was employed in a demonstration model which was based on the single-hinge concept described in the appendix. Another method would be to use synchronized motors. For instance, the example shown in Figure 2 could include motors mounted on each intermediate block. With interlocked gears, each motor would torque and rotate the adjacent ends of the rim segments. Figure 3 is a schema of this motor-driven method.

As indicated in Figure 4, flexible spokes are metered outward as the rim is deployed. Each joint in the rim is supported by two spokes extending to opposite ends of the hub (see Fig. 4). In this arrangement, each pair of spokes, when tensioned, functions as a truss. Each can be kept tensioned throughout deployment. Therefore, these spoke trusses can at all times stabilize each rim joint against forces in either axial or radial directions (relative to the hub axis).

For this arrangement, differential metering of the spokes will be required, as may be noted in Figure 4 from the differing lengths among the spokes during deployment. This will require that the metering mechanism be fairly complex, though not inordinately so.

The hub of the structure may have several functions. One that it must have is to form, along with the spokes, the structural trusses. Since the spokes will be tensioned, the hub, as well as the rim, will be compressed. The length of the hub may depend on design constraints, but its proportion to the lengths of the spokes will have a large influence on the truss stiffness. As shown later in this report, the stiffness of the trusses against deflection in the direction of the hub axis increases greatly as the length of the hub is increased.

Other functions of the hub may be to provide support for the whole structural assembly during launch, to house the spoke reels and their mechanisms, and to accommodate stowage of the equipment that the deployed structure will eventually support.

Applications

This generic, spoked-wheel structure might be used to deploy and support any of the following types of large-area equipment:

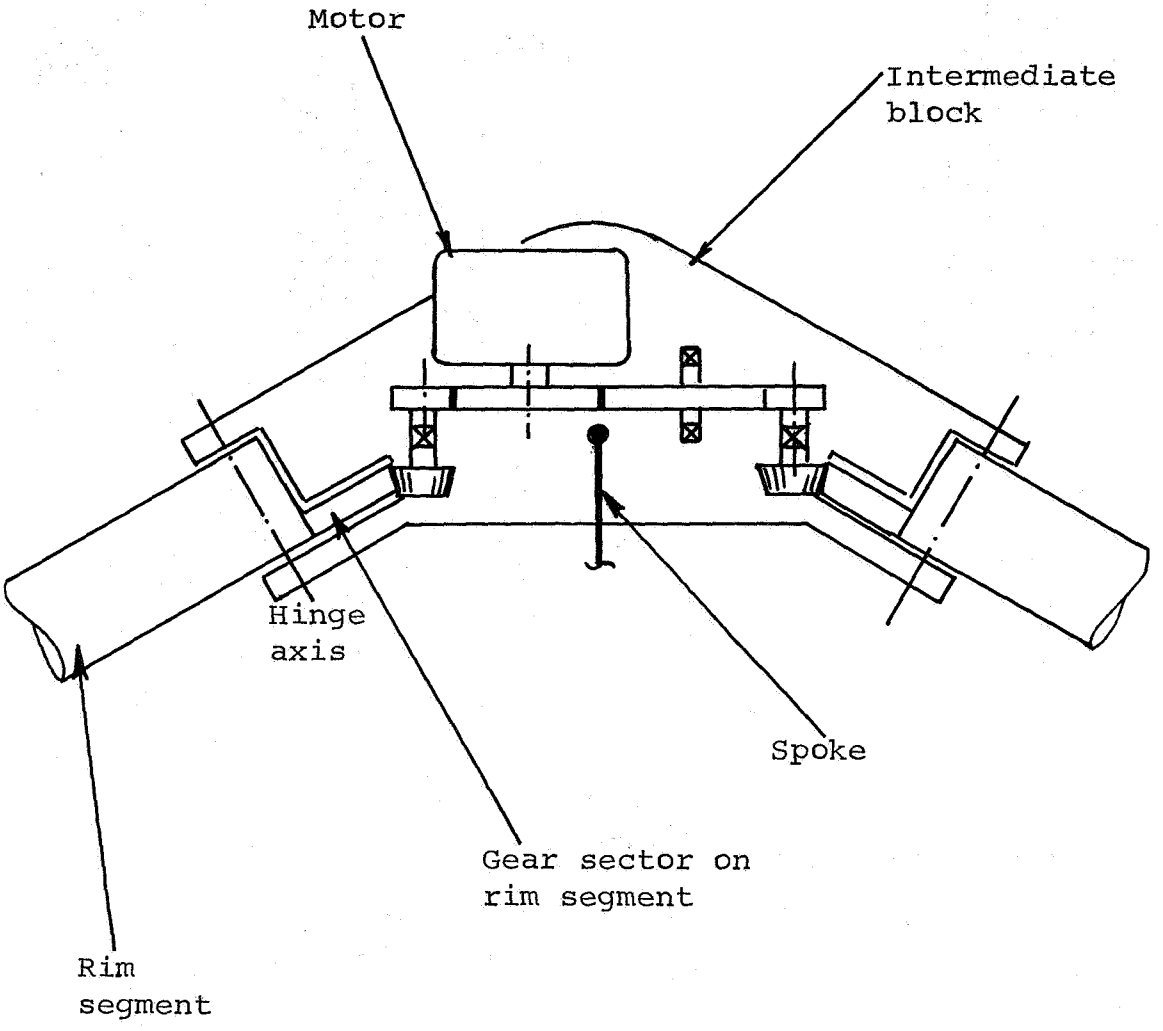

Figure 3. Scheme for Motor-Driven Rim Deployment

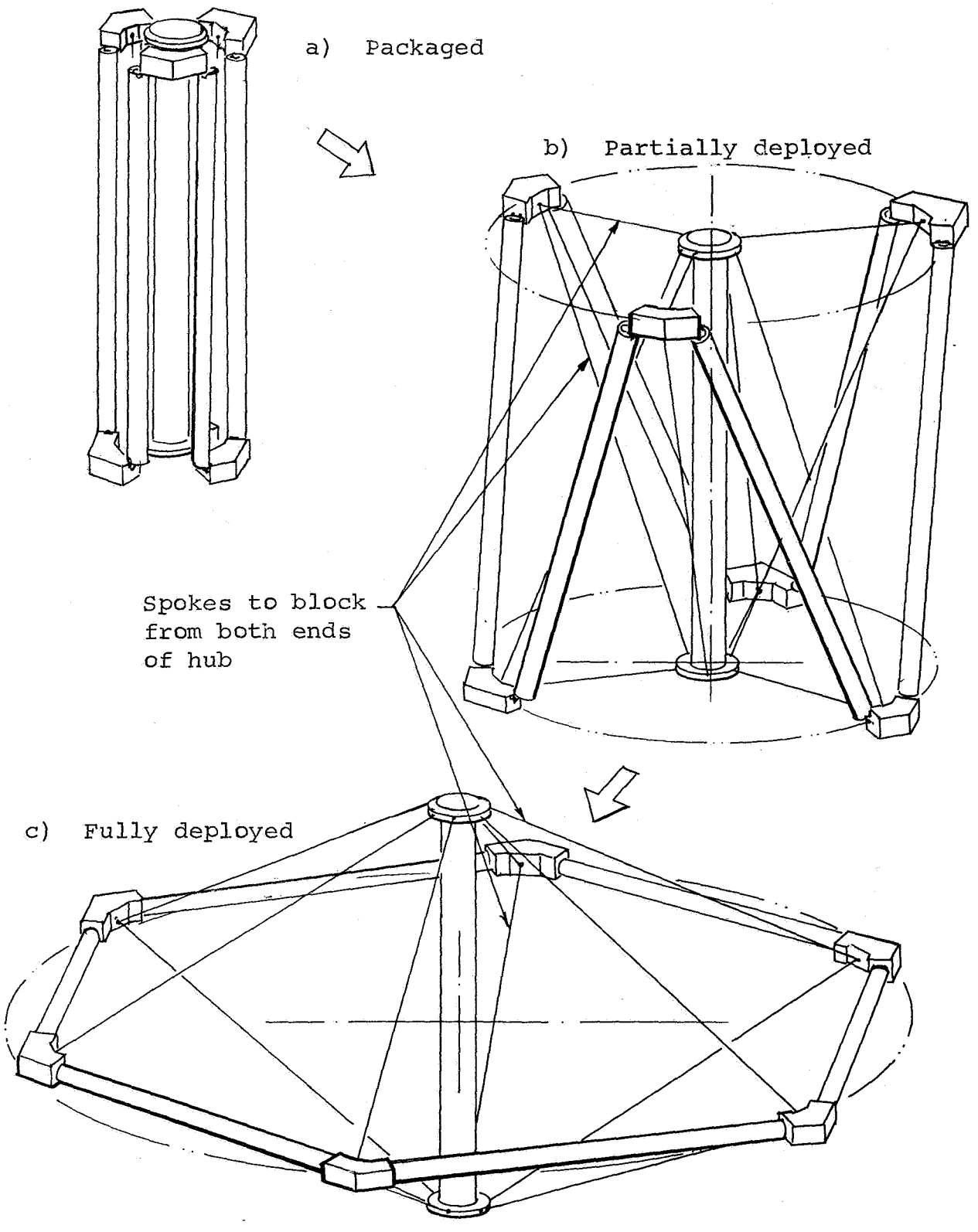

Figure 4. Deployable Rim with Spokes and Hub

1) Reflecting surfaces for antennas or solar-energy collectors and concentrators

2) Radio-frequency lenses

3) Solar-irradiation shades

4) Micrometeorite shields

5) Solar-cell arrays

In general, if they are to be deployed, such surfaces or arrays as these must be furlable, foldable, or otherwise compactable. If so, they can be stowed on or about any or all of the structural components (i.e., rim segments, spokes, or the hub). Deployment of these surfaces or arrays would usually accompany deployment of the structure so that both deployments occur synchronously and employ the same mechanisms.

Some of the following methods of attaching and deploying the equipment listed above have been considered.

Reflecting surfaces.- For parabolic antenna dishes, conducting screens on rigid parabolic ribs (based on the concept developed by Lockheed for the NASA Applications Technology Satellite) could be deployed and supported by the spoked wheel. With the outer ends of the ribs supported by the rim, and the inner ends supported by the hub, thermal distortions of the ribs would be greatly reduced.

Also, the spoked-wheel concept can be used to deploy and support a paraboloid-shaped mesh, formed by attaching with "drop-cords" the mesh to the spokes. This concept is investigated in Reference 5.

A third application, for either an antenna dish or a solar-energy collector, consists of using the present structural concept to deploy and support a conical surface. Such a surface can be stowed by elastically wrapping it about the hub. The cone, used as an antenna, would reflect rays to a secondary, smaller, rigid surface which would focus the rays. This concept of a conical and a secondary reflector has been investigated by the Jet Propulsion Laboratory, as reported in Reference 6.

Radio-frequency lenses.- The amount of gain that can

be achieved by increasing the size of a reflector antenna is usually limited by the rms path-length error that results from geometric imperfections in the reflector surface. Ruze, in Reference 7, derived the following approximate formula for the actual gain γ of a circular antenna with a filled aperture:

$$\gamma = \eta \, \gamma_o \exp \left[-\left(2\pi \frac{\delta}{D} \frac{D}{\lambda}\right)^2\right]$$

where γ_o = gain for the ideal antenna

η = aperture efficiency factor accounting for all sources of loss except those due to surface imperfections that affect path length

D = aperture diameter

λ = wavelength of electromagnetic radiation

and δ = rms value of error in phase at the aperture plane, measured in distance

For a standard paraboloidal reflector, the value of δ is approximately equal to twice the rms surface imperfection (as measured by the amplitude of geometric deviations from the ideal reflector shape). For a given type of reflector construction, this rms surface imperfection tends to be directly proportional to the aperture diameter. Accordingly, δ/D in Ruze's formula is approximately constant. Therefore, for a given value of λ, the formula shows that gain can be increased only to a certain maximum value by increasing D; further increase in D only decreases the gain.

This size limitation can be avoided by using a lens-type antenna. With a lens, phase synchronization at the aperture plane is achieved, not by equalizing path length, but by delaying phases of the rays by varying degrees over the aperture. Optically, this is accomplished by a shaped, transparent dielectric. For radio-frequency wavelengths, appropriate dielectrics, such as foamed plastics, can similarly be used. For large apertures, however, the weight and storage volume can be greatly reduced by utilizing an array of lightweight, phase-delaying electronic devices, either passive or active (i.e., an artificial

dielectric). The position of each device is not extremely critical; it is only necessary that the device intercept most of its assigned rays and accurately delay their phase. Thus, arrays (apertures) of such devices can be of a larger aperture than can reflectors and still avoid severe loss of gain due to geometric imperfections.

One method of providing such a lens-type antenna for space is to mount the array of phase-delaying devices (which now function as an artificial, shaped dielectric) on a flexible blanket. The blanket could be packaged on the spoked-wheel structure, and subsequently be deployed and tensioned by the spoked wheel into a flat plane, a conical shape, or another suitable shape. This packaging and deployment could be accomplished by methods similar to those detailed later for solar-cell arrays mounted on blankets.

Solar-irradiation shades and micrometeorite shields.- Large shades and shields may be considered for various uses. For instance, shades have often been considered for limiting solar irradiation of cryogenic fuels during their stowage in space. Experimental and military equipment might pose similar requirements for large shades or shields. Key problems in meeting such requirements, however, are to provide a minimum-weight surface and to support it with a structure stiff enough to allow control of its orientation.

In these cases, the shading or shielding surface would be segmented into gores which could be furled either about the hub or about the rim segments of the spoked wheel. They would then be unfurled from those components and tensioned between the rim segments and the hub as the wheel is deployed. This same method of deploying planar surfaces, as it applies to solar-cell arrays, is described below in greater detail.

Solar-cell arrays.- There is well-publicized speculation regarding space deployment of extremely large arrays of solar cells for the purpose of generating electrical power for domestic usage. Whether such a method is economically feasible is doubtful unless major technological advances are made in a number of areas, including that of deployable structural design. Large solar-cell arrays are also being considered, however, to fulfill growing power requirements for space equipment. Arrays have proven to be a feasible way of satisfying this requirement.

Large blankets of solar cells could be fabricated in gores

and, as noted previously, stowed for launching by being furled about the hub or rim segments. For smaller arrays, the hub might be designed to have a sufficient diameter so that the gores could be furled about it. But for larger arrays, the rim segments might be sufficiently large so that the gores could be individually furled about them. This latter scheme is depicted in Figure 5, where the wheel is shown partially deployed. An eight-sided rim is shown in that figure only for the sake of clarity in presenting the concept. The same system is shown fully deployed in Figure 6.

One of the principal requirements of an array of solar cells is that it be kept sun-oriented so that it can efficiently generate electricity. A control system maintains the orientation, and, generally, the maximum frequency to which the control system responds is smaller than the lowest, fundamental, natural vibrational frequency of the structure. Resonances and adverse interactions between the structure and the control system are thus avoided.

However, demands for structures to support large areas, and demands to minimize the weight of such structures, will tend to cause the vibrational frequencies of the system to be lowered. As a result, the requirement that the vibrational frequencies be greater than the control frequency dominates the structural design. To meet this requirement with boom-deployed arrays (see Refs. 1, 2, 3 and 4), the rectangular blankets are tensioned between bars, resulting in compression of the booms that hold the bars apart. For an array deployed by a spoked wheel, the blanket gores would also be tensioned, and this would induce rim compression.

In this case of a spoked-wheel structure, blanket tension could be applied and maintained in several ways, either during or after deployment of the structure. For example, a negator or other types of springs could be employed to resist unrolling of the gores from the hub or rim segments; or halyards attached to the gores could deploy and tension them after rim deployment.

In any tensioning scheme, equilibrating compression forces would be induced in the rim of the spoked wheel; and the rim, spokes, and hub must be designed to withstand those induced forces. That procedure is given in the following section which presents design analyses for solar arrays.

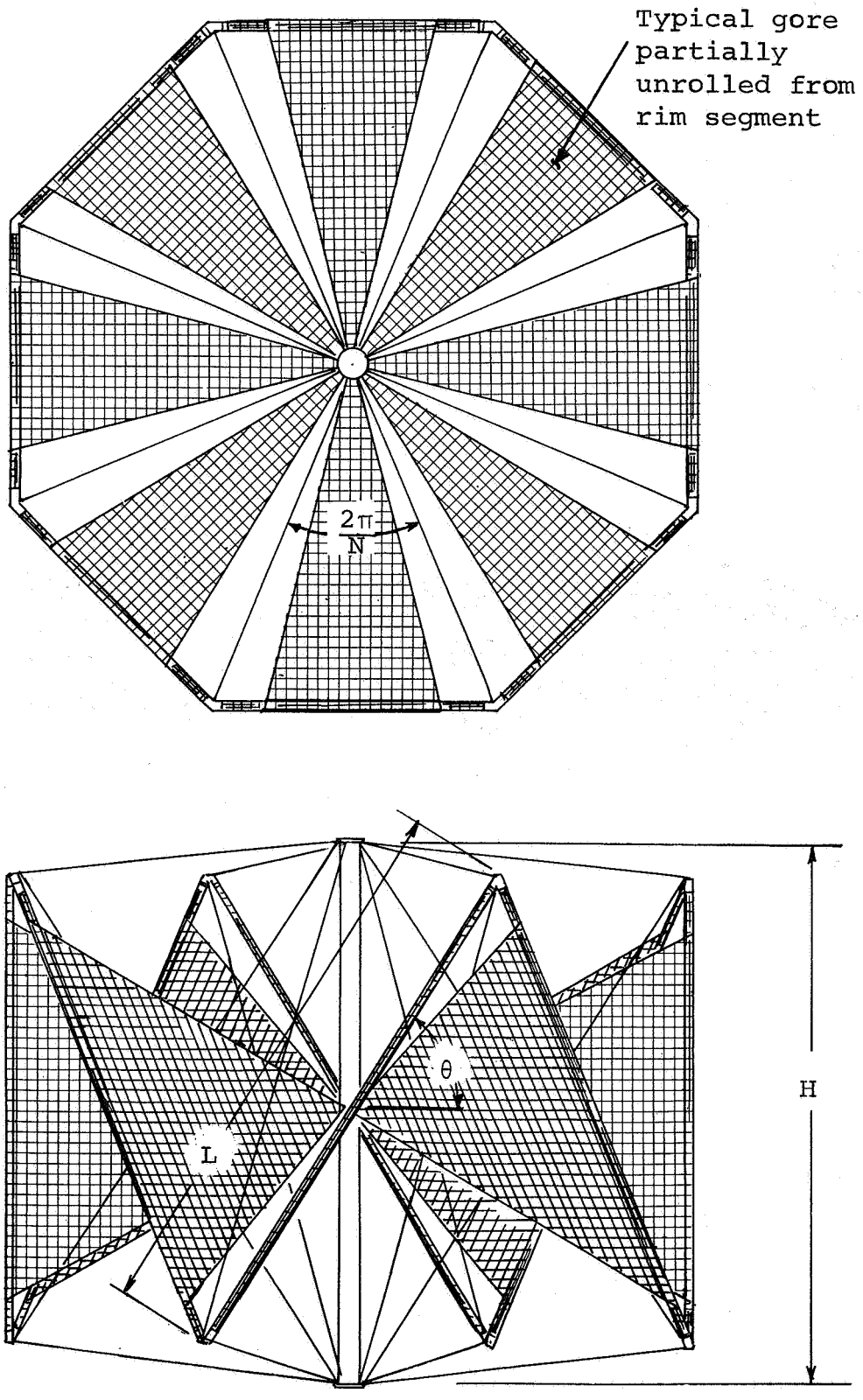

Figure 5. Solar-Cell Gores Partially Deployed by Spoked-Wheel Structure

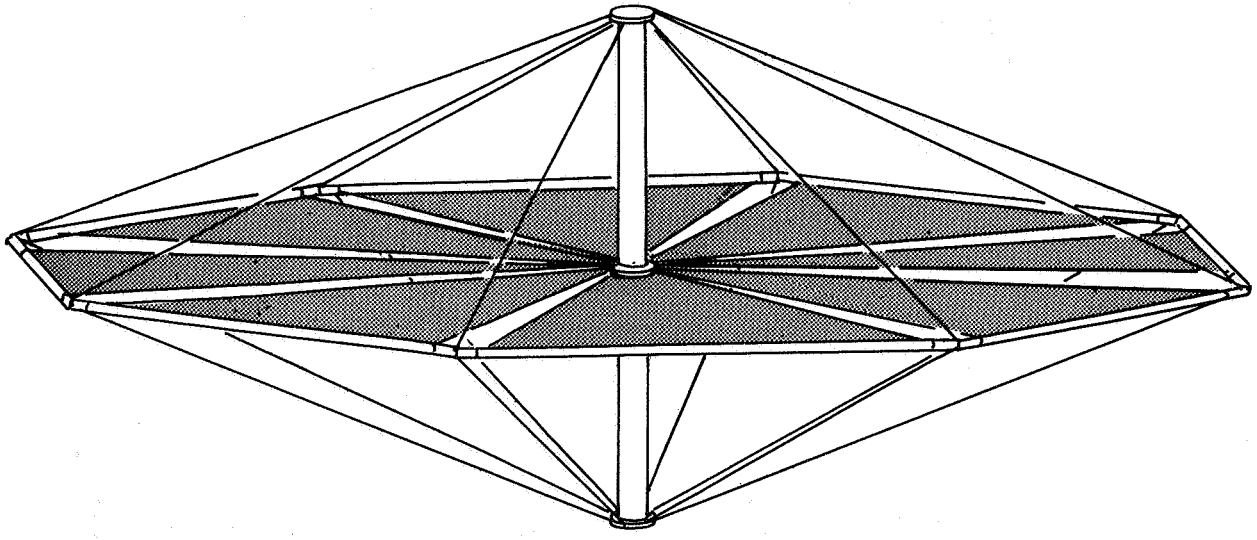

Figure 6. Solar-Cell Gores Fully Deployed by Spoked-Wheel Structure

DESIGN ANALYSES FOR SOLAR ARRAYS

A parametric design analysis is summarized below. From it, structural weight fractions are calculated for the spoked wheels which support solar-cell arrays. These structural weight fractions G are defined as:

$$G = \frac{W_S}{W_S + W_A}$$

where W_S = total structural weight of the spoked wheel

W_A = total weight of the solar-cell blankets in a system

Assumptions

The following general assumptions are made in this analysis:

1) The general structural configuration and method for stowing and supporting the triangular blankets (gores) of solar cells are shown in Figure 5, and the number of gores N can be any even integer that is greater than or equal to four (4).

2) The length of the hub of the spoked wheel is equal to the length of the rim segments (L = H in Fig. 5); and lengths of the rim segments, spokes, and hub are calculated as though they were lines of no thickness.

3) Each gore of the array is tensioned throughout deployment by the amount necessary to maintain a constant vibrational frequency.

4) Gore tensions are supplied by the deploying torques applied to the rim-segment hinges.

5) Each pair of spokes attached to a hinge point is tensioned by an amount approximately equal to the gore tension, which is also supplied by the deploying torques.

6) The design of all the structural components of the

spoked wheel is governed by the requirements placed on their stiffness rather than on the strength of their materials.

7) The total structural weight of the spoked wheel is the sum of the weights of the four components (rim segments, spokes, motor-plus-block assemblies, and the hub).

8) The blanket gores are stored on the rim segments.

Additional assumptions are noted in the following summary of the analysis.

Blanket Tension Requirement

Figure 7 shows a partially deployed gore of the solar-cell blanket; it is seen that during deployment

$$x = \frac{L}{2} \frac{\cos \theta}{\tan \frac{\pi}{N}}$$

and

$$\ell = 2x \tan \frac{\pi}{N}$$

where all of these symbols are defined by the dimensions in Figures 5 and 7.

It is assumed that for purposes of calculating the vibrational frequency of a gore, the gore acts as a string whose weight per unit length varies linearly along its length. For a rim-stored gore, the value of the weight per unit length at the rim is:

$$w = mg\ell$$

where m is the blanket mass per unit area and g is the acceleration due to gravity. The fundamental vibrational frequency of such a string can be approximated as:

$$f^2 = \frac{Tg}{2wx^2}$$

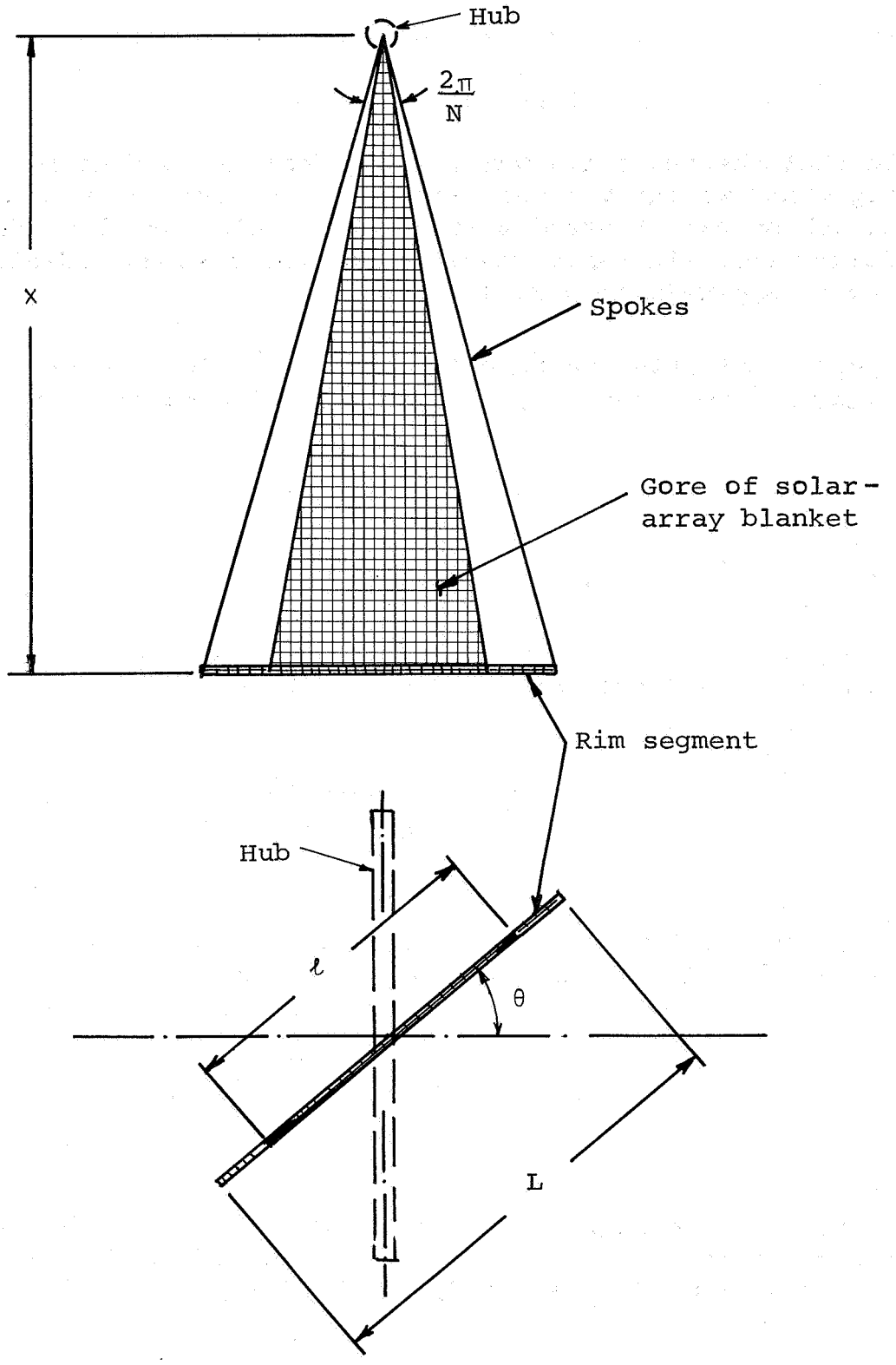

Figure 7. Partially Deployed Gore of Blanket and Segment of Support Structure

where f = vibrational frequency

and T = tension in the gore

(Note that the above frequency is equivalent to that for a uniform string whose weight per unit length is the same as that at the midlength of this tapered string. Also note that this frequency is larger than the exact solution for the assumed, idealized string by approximately 3%.)

By substituting in this frequency equation the previously given expressions for w, χ, and ℓ, the equation becomes:

$$f^2 = \frac{2T \tan^2 \frac{\pi}{N}}{m L^3 \cos^3 \theta}$$

The length of a rim segment L is related to the total area of the array A and the number of gores N by:

$$L = 2\sqrt{\frac{A}{N} \tan \frac{\pi}{N}}$$

By substituting the expression for L into the frequency equation, the blanket tension is determined as:

$$T = \frac{4m f^2 A^{3/2} \cos^3 \theta}{N^{3/2} \tan^{1/2} \frac{\pi}{N}}$$

Thus, the tension required to maintain a constant vibrational frequency increases throughout deployment; i.e., T increases as θ goes from 90°, packaged, to 0°, fully deployed.

Forces and Moments on the Structure

Figure 8 shows the forces on a rim segment during deployment, and indicates that the radial component of the tensions in each pair of spokes is assumed equal to the gore tension. The number of gores that should be used in an efficiently designed system will be shown later to be sufficiently large to warrant the use of the following approximation in calculating the rim compression and rim moment:

$$\sin \frac{\pi}{N} \approx \tan \frac{\pi}{N} \approx \frac{\pi}{N}$$

and

$$\cos \frac{\pi}{N} \approx 1.0$$

Then circumferential radial force C (see Fig. 8), necessary to equilibrate the tensions, is:

$$C = \frac{TN}{\pi}$$

The corresponding axial compression in a rim segment P is:

$$P = \frac{TN}{\pi} \cos \theta$$

The moments, shown in Figure 8, that must be applied to the rim segments in order to deploy them against the tensions in the gores and the spokes are those necessary to equilibrate the eccentrically acting compressive forces C. Therefore:

$$M = \frac{TNL \sin \theta}{2\pi}$$

By substituting the previous expression for T into the equations for M and P, these moments and forces are found in terms of the independent design parameters m, f, A and N and the deployment parameter θ:

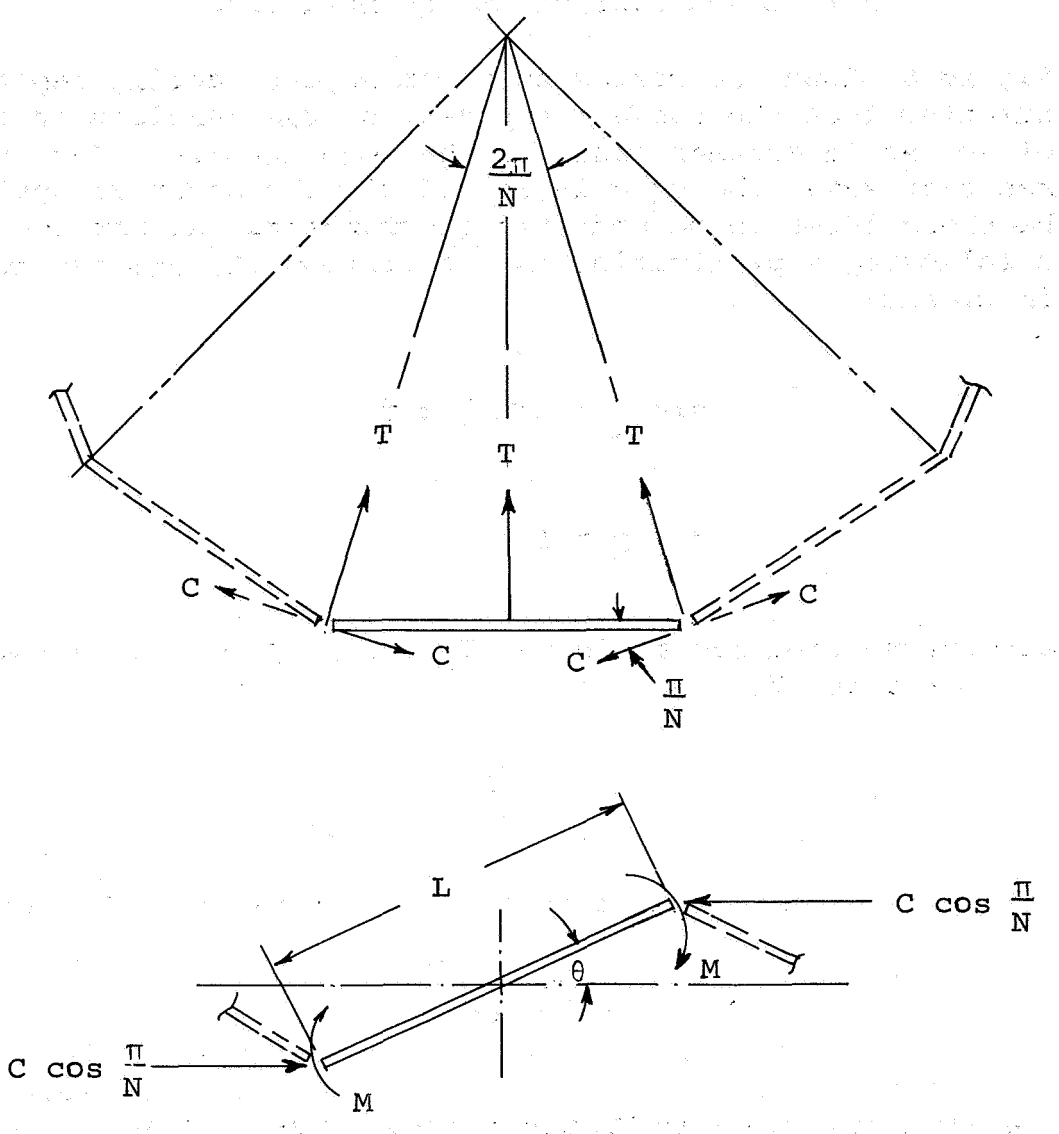

Figure 8. Moments and Forces Acting on a Rim Segment During Deployment

$$P = \frac{4m\, f^2\, A^{3/2} \cos^4 \theta}{\pi\, N^{\frac{1}{2}} \tan^{\frac{1}{2}} \frac{\pi}{N}}$$

$$M = \frac{4m\, f^2\, A^2 \cos^3 \theta \sin \theta}{\pi N}$$

The maximum value of the moment occurs at $\theta = 30°$, where:

$$M_{MAX} = \frac{3\sqrt{3}\, m\, f^2\, A^2}{4\pi N}$$

The maximum value of P occurs at $\theta = 0°$; however, at $\theta = 30°$, P is 9/16 of its maximum value.

Designs and Weights of Structural Components

Rim segments.- The rim segments are assumed to be circular, cylindrical aluminum tubes, and they must withstand the previously calculated loads. They are designed according to elastic stability considerations (which is consistent with the general assumption that material strength does not govern their design). The diameter of a rim-segment tube and the thickness of its walls are designed so that under the maximum bending moment the tube walls will not buckle locally, and under maximum axial loading the tube will not buckle in the Euler mode. In calculating this Euler-buckling mode of failure, the ends of the tube are assumed to be simply supported, that is, free to rotate but not to deflect. The two loadings are not assumed to act simultaneously, but the tubes are proportioned so that the magnitude of each type of loading is half of its respective ultimate buckling strength.

Accordingly, the bending moment on a tube is equated to half of its bending strength, giving:

$$M = 1/2\ \pi R^2\, tk\, E_R \frac{t}{R}$$

where R = tube radius

t = tube wall thickness

k = buckling coefficient

E_R = Young's modulus of tube material

Equating the compressive load to half the Euler strength gives:

$$P = \frac{\pi^3 E_R R^3 t}{2L^2}$$

The weight of a rim segment W_R is:

$$W_R = 2\pi \rho_R LRt$$

where ρ = density of tube material

These last three equations can be combined into an equation which relates W_R, P and M, while eliminating t and R. When the foregoing expressions for the maximum bending moment, the axial load, and the blanket tension are substituted into that equation, the following equation is obtained:

$$W_R = 0.01627 \left(\frac{mf^2A^3}{N^3}\right)^{3/5}$$

In this equation the following substitutions are also made:

$k = 0.1$ (conservative value, see Ref. 8)

$\rho_R = 172.8$ pcf (pounds per cubic foot) for aluminum

$E_R = 1.44 \times 10^9$ psf for aluminum

(Note that pound and foot units are used for these properties because the weight equation is later evaluated for the other parameters in terms of the same units.)

Spokes.- The spokes are taken to be steel tapes, and their design is governed by the elastic constraint they must provide in order to prevent the compressed rim segments from buckling as a hinged linkage. In this buckling mode, the joints of the rim segments are assumed to hinge freely, so that these joints could, if unconstrained, displace in the direction of the hub axis. Therefore, the compressed rim segments depend upon the truss stiffness of the spokes to prevent such buckling. Since the axial compression of the rim is at a maximum and the truss stiffness at a minimum when the rim is fully deployed, the spokes are sized for that condition.

The stiffness ψ of a truss formed by a pair of spokes is readily found as:

$$\psi = \frac{4\, A_{SP}\, E_{SP}\, \sin^3 \frac{\pi}{N}}{L}$$

where A_{SP} = cross-sectional area of one spoke

E_{SP} = Young's modulus of spoke material

and where the hub length is equal to the length of a rim segment, as assumed initially.

The buckling strength P_{CR} of the compressed and hinged rim segments (assumed rigid between hinges) is shown in Reference 9 to be:

$$P_{CR} = \frac{\psi L}{4}$$

Therefore

$$P_{CR} = A_{SP}\, E_{SP}\, \sin^3 \frac{\pi}{N}$$

The weight of one spoke W_{SP} is:

$$W_{SP} = \frac{\rho_{SP}\, A_{SP}\, L}{2 \sin \frac{\pi}{N}}$$

By making $P_{MAX} = 1/2\ P_{CR}$; by combining the foregoing equations for W_{SP} , P_{MAX} , and T ; and by using the previous small-angle

approximation for $\sin \frac{\pi}{N}$, the weight of a spoke is determined as:

$$W_{SP} = 3.11 \times 10^{-9} N^3 m f^2 A^2$$

In this equation the following substitutions are made (for steel):

$$\rho_{SP} = 518.4 \text{ pcf}$$

$$E_{SP} = 4.32 \times 10^9 \text{ psf}$$

Motor.- From sales literature on electrical motors for space applications, and from design considerations of the intermediate blocks between rim segments, the following empirical formula was developed for the weight of the motor and block assembly located between adjacent rim elements:

$$W_M = 0.70 M^{1/3}$$

where W_M = motor-assembly weight, pounds

M = design moment, foot-pounds

By substituting into this formula the previous expression for the maximum deployment moment, the motor-assembly weight is determined as:

$$W_M = 0.29 \left(\frac{m f^2 A^2}{N} \right)^{1/3}$$

Hub design.- The hub is assumed to be a circular aluminum tube. It is designed to withstand axial compressive forces acting on it because of rocket launch accelerations. This hub tube is assumed to be a cantilever and it is assumed to be subjected to the inertial forces of all the other components of the system when they are undergoing an acceleration of 25 g's. Accordingly, the axial load on the hub is:

$$P_H = 25 \ (mgA + NW_R + 2NW_S + NW_M)$$

By an optimum design procedure similar to that used by Shanley (Ref. 10), the weight of the hub is determined as:

$$W_H = \left(\frac{4}{\pi ck}\right)^{1/3} \left(\frac{4\pi A}{N^2}\right)^{5/6} \rho_H \left(\frac{2P_H}{E_H}\right)^{2/3}$$

where ρ_H = density of hub material

E_H = Young's modulus of hub material

and where the factor of two (2) before P_H is the result of taking the buckling strength to be twice the applied load. For this aluminum cantilevered tube:

$$k = 0.10$$

$$c = 0.25 \text{ (buckling coefficient for a fixed-free column)}$$

$$\rho_H = 172.8 \text{ pcf}$$

and $$E_H = 1.44 \times 10^9 \text{ psf}$$

The hub weight is then:

$$W_H = 6.43 \times 10^{-3} \left(\frac{A}{N^2}\right)^{5/6} P_H^{2/3}$$

Structural Weight Fraction

The total structural weight of the spoked wheel W_S is calculated by summing the previously formulated component weights:

$$W_S = NW_R + 2NW_{SP} + NW_M + W_H$$

The total weight of the system is then $W_S + W_A$, where $W_A = mgA$.

For a structure designed to support a prescribed payload as well as its own weight, a commonly used index of efficiency is the structural weight fraction designated here by G and defined as:

$$G = \frac{W_S}{W_A + W_S}$$

Values of this index, as well as values of individual component weights, are presented in the following section of this report.

RESULTS AND DISCUSSION

Weights of the structural components and the structural weight fractions G were calculated using the foregoing formulas with the following values for the parameters:

$$A = 10^3 , \ 10^4 , \ 10^5 \text{ and } 10^6 \text{ ft}^2$$

$$N = 10 \text{ to } 40$$

$$mg = 0.30 , \ 0.10 \text{ and } 0.030 \text{ psf}$$

$$f = 0.20 , \ 0.15 , \ 0.10 \text{ and } 0.05 \text{ cps}$$

Figure 9 shows typical weights for the four types of structural components as they vary with the number of gores when the blanket area, the weight per unit area, and the vibrational frequency are fixed. It is clear in this figure that N has a very significant effect on the weights of the individual structural components. With an increase in N , weights of some of the components increase while others decrease. This makes it clear that N has an optimum value that will minimize the total weight of the structural components, and thus minimize the structural weight fractions.

The individual weights of the components vary with N (see Fig. 9) because of a combination of influences which are present in the weight equations. For instance, weights of the rim segments are influenced greatly by the tube strength, which varies as $1/N^2$; however, rim-segment weights are also influenced by their loading, of which bending varies as $1/N$ and compression is invariant with N . The combined result is a decrease in the rim weight when N is increased. Contrariwise, the spoke weight increases when N is increased, largely because the truss stiffness of the spokes varies with the cube of the angle between the two spokes which comprise the truss. That angle is $2\pi/N$ for the assumed proportions $L = H$.

Figure 10 shows structural weight fractions versus N for the three different values of mg when $A = 10^4$ ft^2 and when $f = 0.20$ cps . Optimum values of N , which minimize G , are in the vicinity of 20 or 30 (only even numbers are admissible) for the three blanket densities. Figure 11 is a graph of G versus N for the several different blanket areas. It shows that the

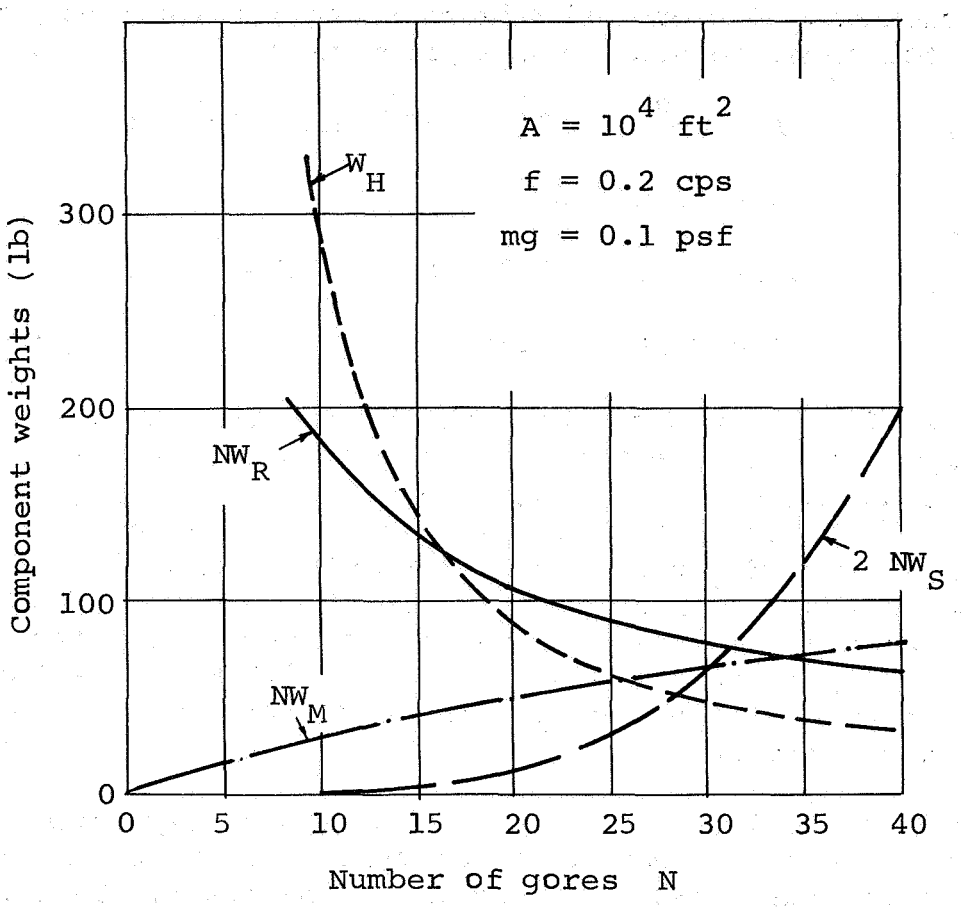

Figure 9. Weights of the Structural Components of the Spoked Wheel Versus the Number of Gores

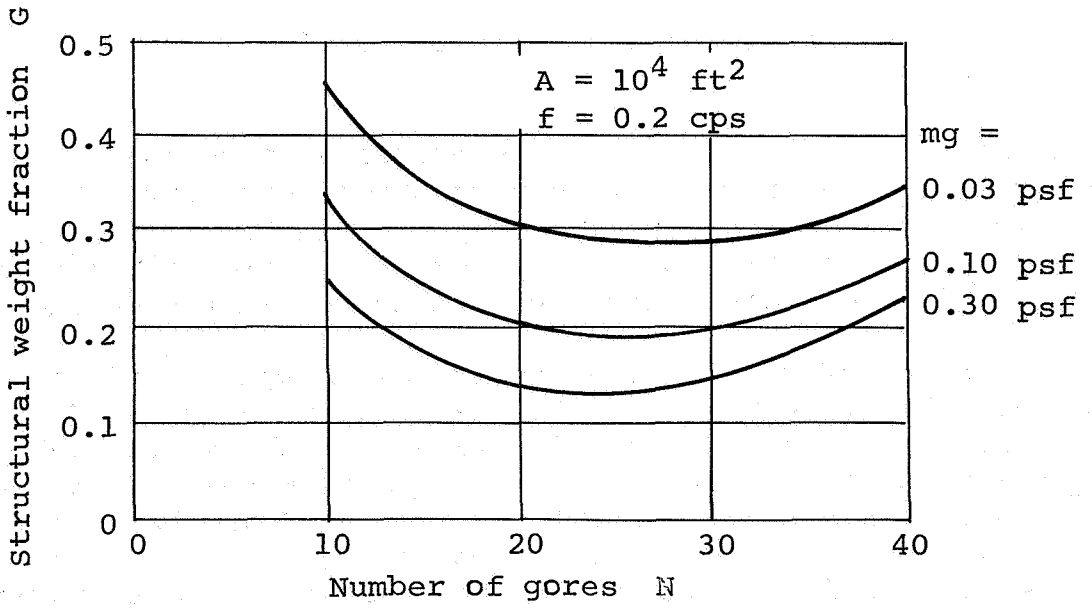

Figure 10. Structural Weight Fractions Versus Number of Gores and Blanket Density; Fixed Area and Frequency

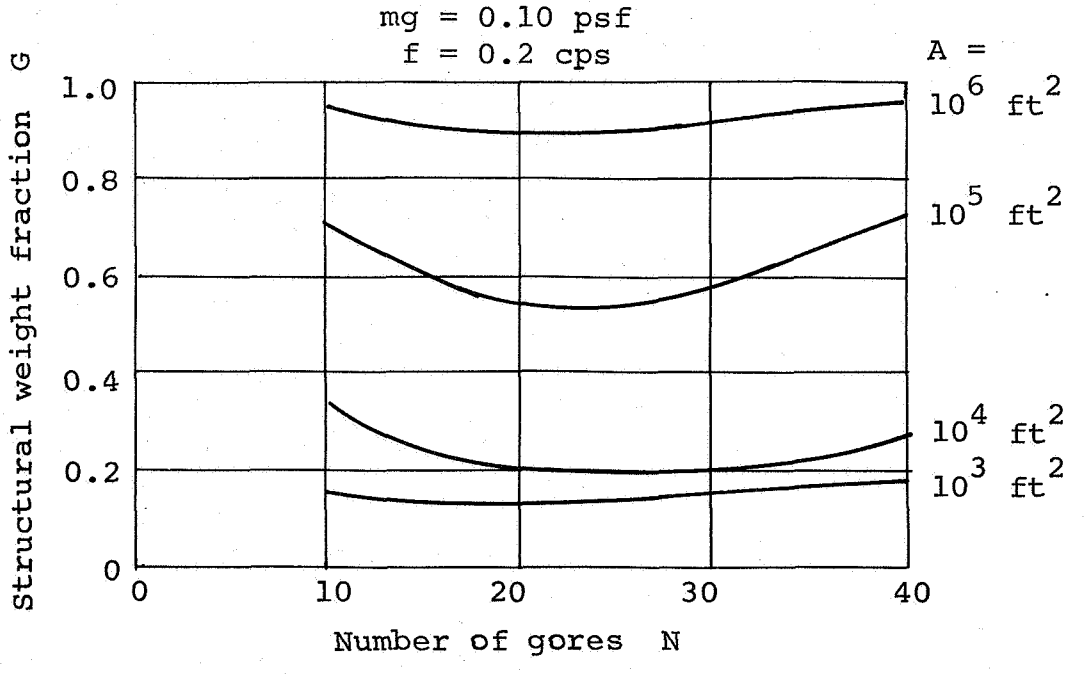

Figure 11. Structural Weight Fraction Versus Number of Gores and Blanket Area; Fixed Density and Frequency

optimum values of N occur in the same vicinity Figure 10 depicts, even when A varies widely.

Accordingly, for a prescribed vibrational frequency, the minimum values of structural weight fractions vary with the blanket area and density. This is depicted in Figure 12, where the weight fractions are seen to increase significantly with both an increase in the blanket area and a decrease in the density.

The effects of varying the vibrational frequency of the system were also investigated. The results are shown in Figure 13, where, for $mg = 0.10$ psf , values of the structural weight fractions are plotted versus frequencies and the area of the blanket. The weight fractions in Figure 13 are the calculated minimum values. These values occur, again, at values of N between 20 and 30. As might be expected, the weight fractions decrease as the blanket frequencies (hence the tensions) decrease.

In Figure 14, the efficiency of electrical power output for the spoked-wheel solar arrays covered by the previous graphs, is plotted against blanket area and vibrational frequency. The efficiency is given in watts per pound of total weight of the structure and the blanket. The calculations in Figure 14 are based on an assumed solar-cell power output of 10 W/ft^2 , and a blanket weight of 0.1 lb/ft^2 . Also shown in Figure 14 are four different solar-array systems: FRUSA (Ref. 1), JPL ① (Ref. 2), LMSC (Ref. 3) (all of which have been fabricated to some extent), and JPL ② which is the preliminary result of a JPL-sponsored study by General Electric entitled Feasibility Study of 110 W/kg Lightweight Solar Array. It is evident from Figure 14 that efficiencies that might be extrapolated for the spoked-wheel systems are much greater than those of the existing boom-deployed designs. However, direct comparison should not be made between the efficiencies of the smaller-area, boom-deployed designs and the spoked-wheel ones. The efficiency that might be extrapolated for a 250-ft^2, spoked-wheel design, for instance, would probably be much greater than can be realized, because motor weights, tube proportions, and spoked sizes would be impractically small. Hence, the spoked-wheel concept should be considered efficient and practical only for larger areas.

The efficiency of the LMSC/NASA system, which is shown in Figure 14, was significantly influenced by the requirement that the system be able to spin. The basis for this requirement was

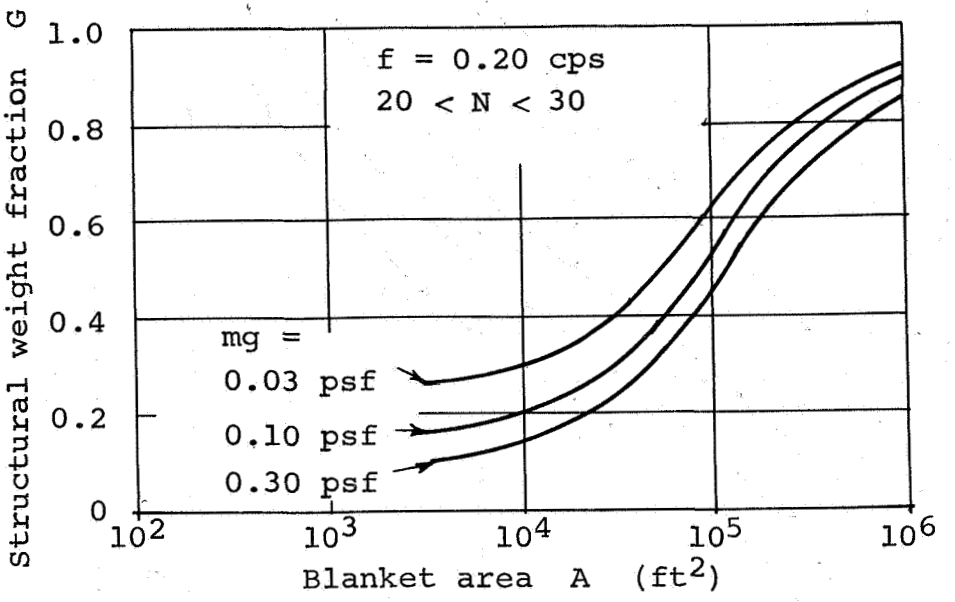

Figure 12. Structural Weight Fraction Versus Blanket Area and Density; Fixed Frequency and Optimum Number of Gores

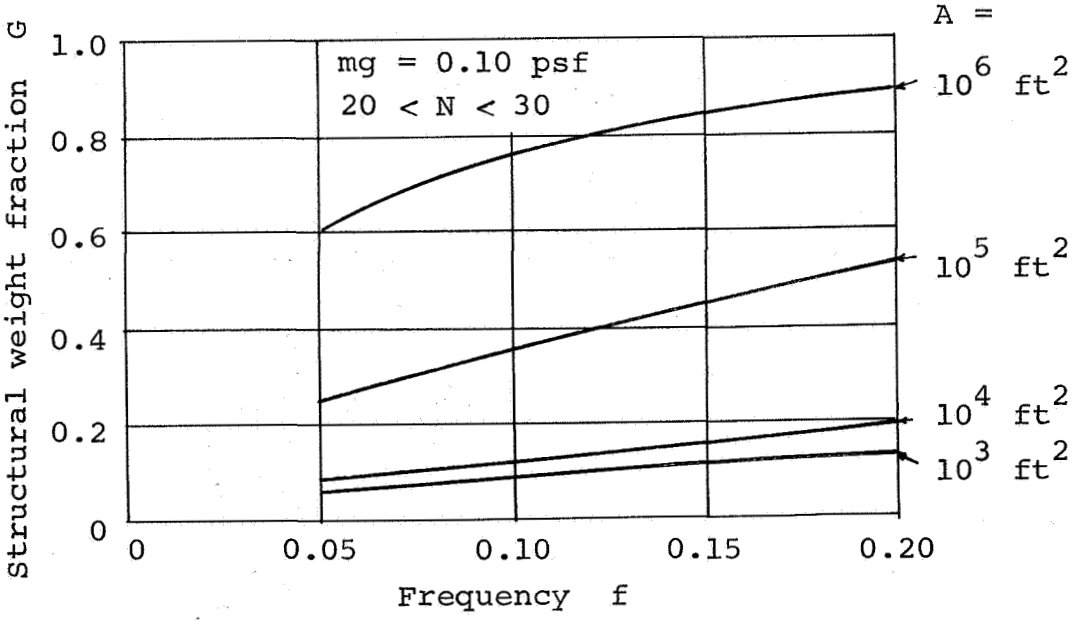

Figure 13. Structural Weight Fraction Versus Vibrational Frequency and Blanket Area; Fixed Density and N

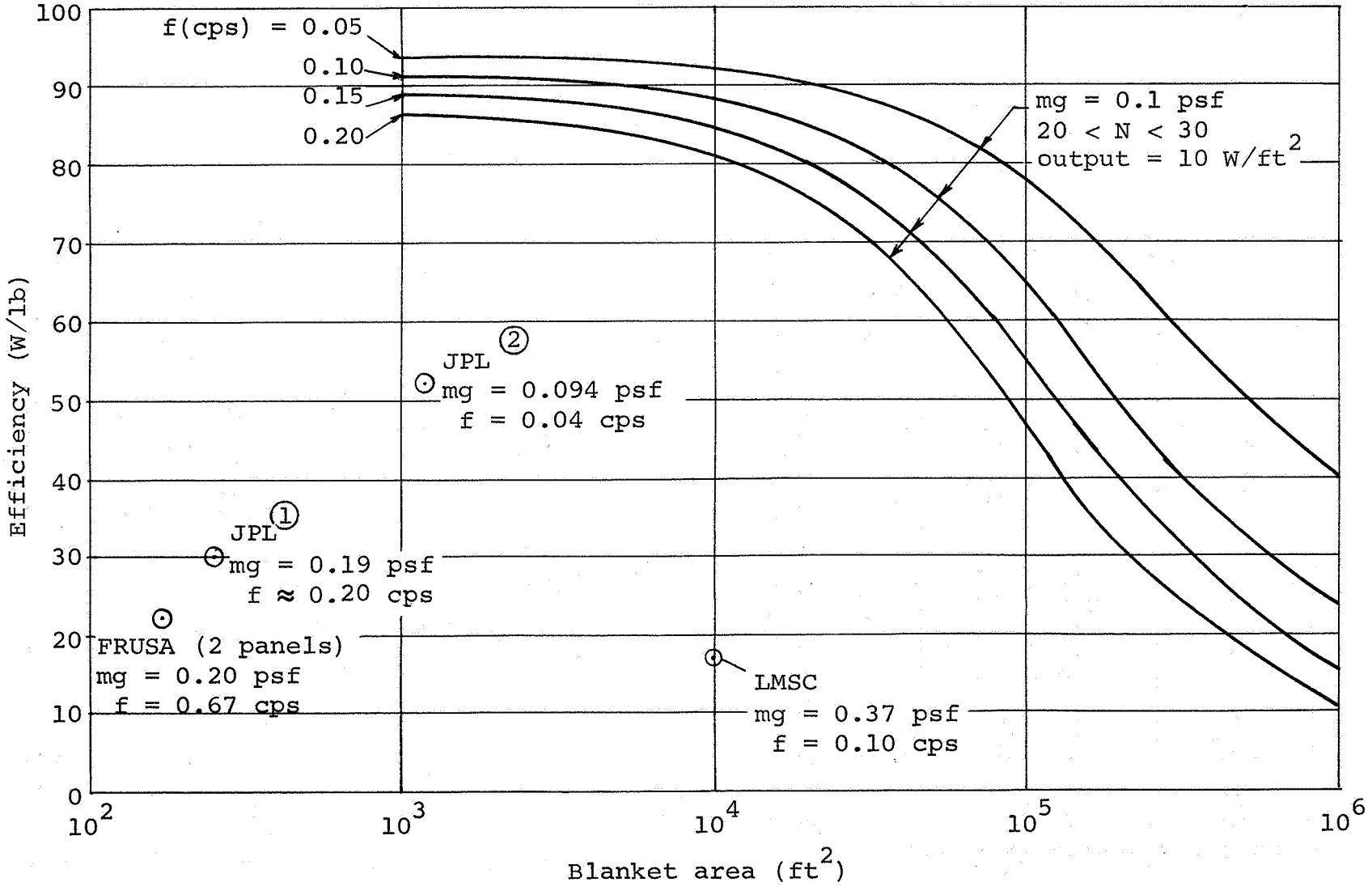

Figure 14. Output Efficiency Versus Blanket Area for Specified Vibrational Frequencies; Fixed Blanket Density, Number of Gores and Power Output per Unit Area

that artificial-gravity experiments would be performed by spinning the space laboratory while portions of its solar arrays were extended. Therefore, its efficiency is somewhat less than if its design had been governed by the same criteria as are applied here to spoked-wheel systems.

The JPL ② system indicated in Figure 14 is the most efficient of all the existing designs. Therefore, it is considered to be a reasonable datum for extrapolating efficiencies for larger systems of that type of boom-deployed, rectangular solar array. That extrapolation is shown in Figure 15 as a plot of efficiency versus blanket area. The following scaling laws, as derived in Appendix B, are used for the extrapolation of the JPL ② system:

$$W_s \alpha fA^{3/2}$$

and

$$f \alpha A^{1/4}$$

Efficiency in terms of watts per pound is related to the structural weight fraction by

$$\text{Efficiency} = (1 - G)100$$

for a 10-W/ft^2, 0.1-lb/ft^2 system. For the above scaling laws

$$G = \frac{1}{1 + \frac{1}{KA^{1/4}}}$$

where K is a constant to be evaluated at the datum. Then

$$\text{Efficiency} = \frac{100}{1 + KA^{1/4}} \text{ (W/lb)}$$

Also shown in Figure 15 is that set of spoked-wheel designs in Figure 14 whose frequencies and areas obey the scaling law

$$f \alpha A^{-1/4}$$

and which, at $A = 10^3$ ft^2, has vibrational frequencies of

0.2 cps. Note that for the blankets of all these spoked-wheel designs, mg = 0.10 psf , and the power output is 10 W/ft^2. It is clear from comparison with the spoked-wheel and boom-supported performance data shown in Figure 15 that the spoked wheel remains much more efficient through the indicated range. Note also that the difference in efficiency would be even greater if the frequencies of the two systems were the same at the 1000-ft^2 datum of each.

It is reemphasized that the spoked-wheel design data presented in the foregoing graphs are based on a number of simplifying assumptions, i.e., that the hub has the same length as a rim segment; that both the hub and rim are monocoque tubes; and that the hub, as a column, supports practically the entire system weight under 25-g launch loads. For very large area arrays these results can lead to impractical designs; for instance, for $A = 10^6$ ft^2 , the tube length becomes very long at $L \cong 120$ ft. Both the tube lengths and weights could be significantly reduced by incorporating stiffened tube designs and by lengthening the hub (possibly by using a deployable boom as a hub). Therefore, for areas of 10^6 ft^2 and larger, a shift in the structural technology is again recommended. That is, spin stiffening might be used, or multiple spoked wheels with tetrahedral interconnected structures might prove more practical than a single spoked wheel. Another solution for very large areas might be the Heliogyro concept (described in Ref. 12) which spins and utilizes solar pressure for attitude control.

An example one-megawatt design of the spoked-wheel system was considered which had the following properties:

$$A = 10^5 \text{ ft}^2$$

$$mg = 0.1 \text{ psf}$$

$$N = 30$$

$$\text{output} = 10 \text{ W/ft}^2$$

Using the datum of $f = 0.2$ cps at $A = 10^3$ ft^2 , the previously cited relationship between blanket area and vibrational frequency gives

$$f = 0.063 \text{ cps}$$

From Figure 15, the output efficiency of this system is seen to be about 74 W/lb. From the design formulas presented previously, the rim-segment weight is calculated as:

$$W_R = 40.46 \text{ lb}$$

or

$$NW_R = 1214 \text{ lb}$$

The spoke weight is:

$$W_{SP} = 10.35 \text{ lb}$$

or

$$2NW_{SP} = 621 \text{ lb}$$

A motor weight is:

$$W_M = 4.65 \text{ lb}$$

or

$$NW_M = 139.5 \text{ lb}$$

And the hub weight is:

$$W_H = 1460 \text{ lb}$$

The total weight of the system, including the 10 000-lb blanket, is then:

$$W_{TOTAL} = 13\ 435 \text{ lb}$$

A rim segment and the hub have a length of:

$$L = 37.4 \text{ ft}$$

The diameter of a rim segment is about 3.2 in, and its wall thickness is about 0.090 in. A blanket tension of about 29.3 lb is required for a vibrational frequency of 0.063 cps. That tension also induces in the rim segments a maximum bending moment of 17 000 ft-lb and a maximum axial compression of 280 lb. The hub diameter is about 30 in. and its wall thickness is about 0.30 in.

For these loads and component sizes, none of the stresses are excessive.

A sketch of this example design in its packaged and deployed

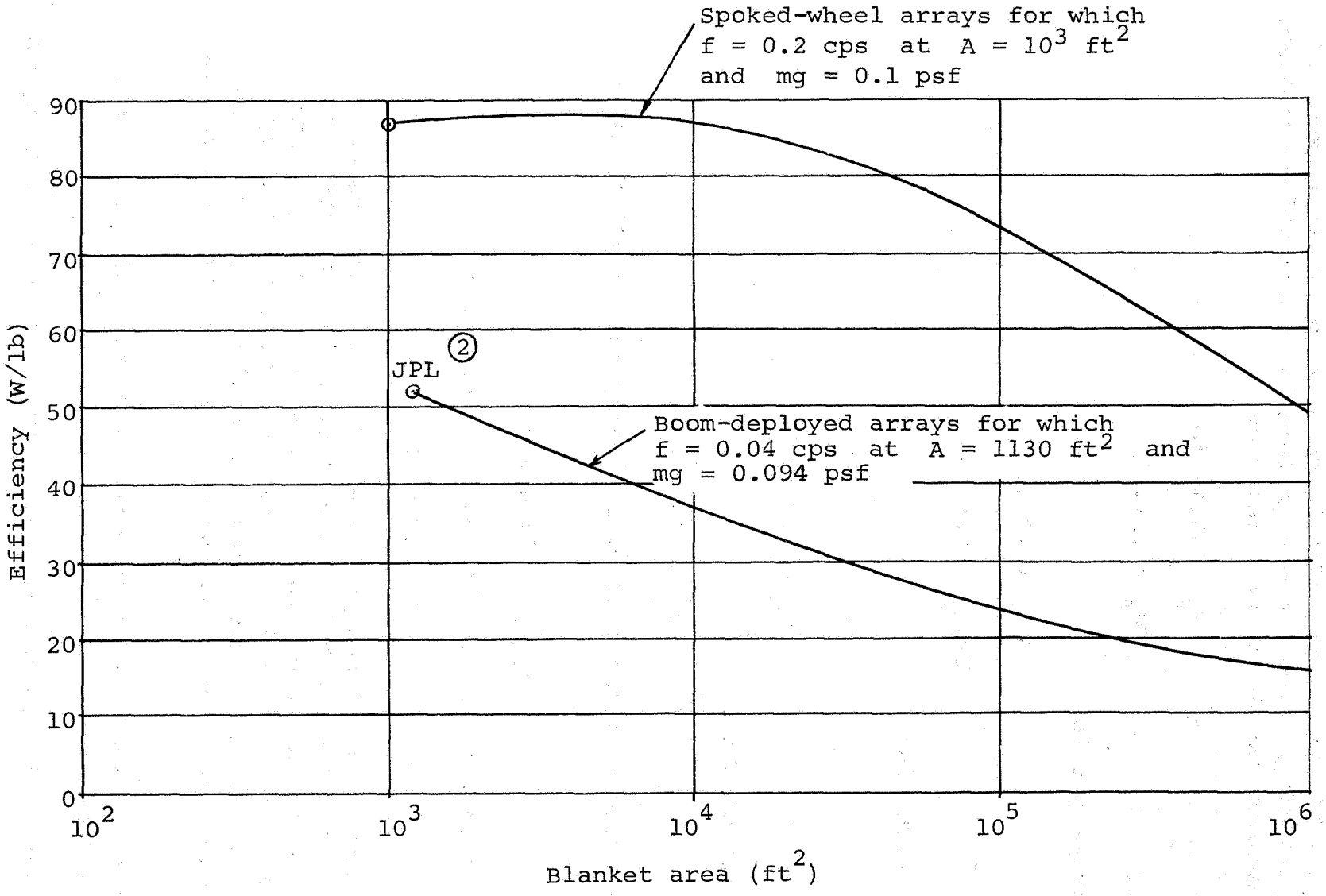

Figure 15. Output Efficiencies for Spoked-Wheel and Boom-Deployed Solar Arrays Versus Blanket Area

configurations is shown in Figure 16. The hub as shown in this figure has a diameter of 60 in. (enlarged from the calculated 30 in.) to accommodate reels and other mechanisms for operating the system. When packaged, the system is seen to be small enough for Space Shuttle launch. Note that the blankets could have been designed to wrap about the hub, and this would have made an even more compact retracted package. Note also that for Space Shuttle launching, the hub could be designed to be much lighter.

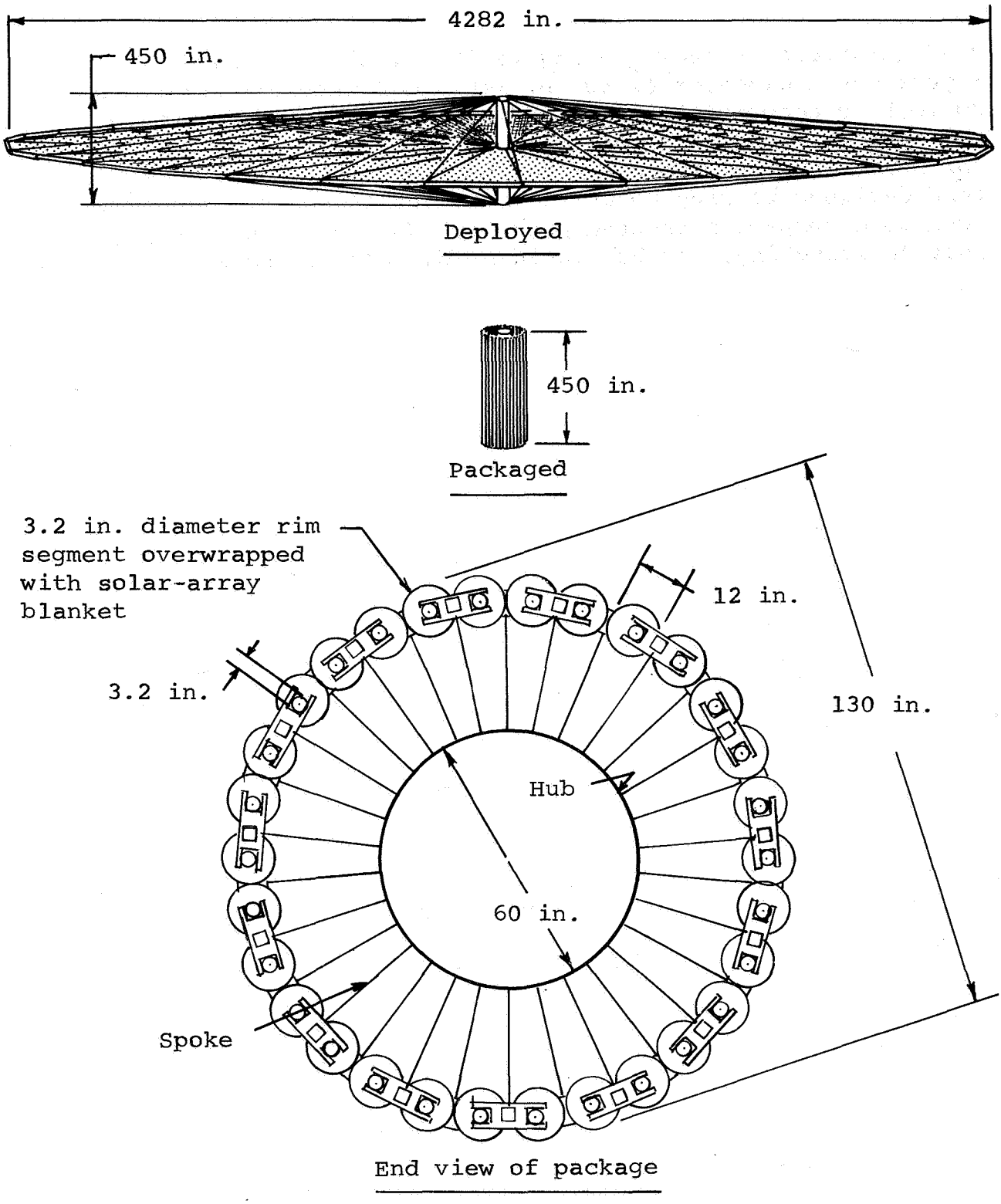

Figure 16. One-megawatt, 10^5-ft^2, Spoked-Wheel Solar Array

CONCLUDING REMARKS

The preliminary design study for deploying large solar arrays with spoked-wheel structures shows that these spoked-wheel designs are substantially more efficient for deploying large arrays than are designs which employ booms. This advantage is shown, even though the present design analysis incorporates assumptions that are probably unduly conservative, since:

1) A smaller safety factor than 2.0 between loads and buckling strengths might be used.

2) The assumed spoke pre-tension might be reduced, in order to reduce the rim loads and, accordingly, the rim weights.

3) Especially for very large arrays, the rim segments and hub should be of stiffened constructions rather than the assumed unstiffened tubes.

4) When deployed, the hub could be much longer if made a deployable boom. As a result, the spokes could more efficiently provide stiffness for stabilizing the rim, and the hub itself could be of a lighter weight.

The deployable spoked-wheel structure is a feasible and practicable concept, and appears to have excellent potential for deploying large-area equipment that must be structurally manageable. Further investigation seems warranted for use in such applications as antennas, reflectors and other equipment requiring the deployment of very large surface areas.

APPENDIX A

DEPLOYMENT OF A SEGMENTED RIM WITH ONE HINGE PER JOINT

Introduction

The main text has described the design and deployment kinematics for the segmented rim of a spoked wheel designed to have two hinges per joint between rim segments. However, it is also kinematically possible to deploy a segmented rim which has only one hinge per joint. In the one-hinge design, the packaged and fully deployed configurations of the rim are the same as those for the concept utilizing two hinges; however, the deployment kinematics are different. Potentially, this one-hinge concept has manufacturing advantages over the two-hinge concept.

The investigation presented here determines how the one-hinge design should be oriented and defines the rim motions that occur during deployment.

Analysis

Some characteristics may be deduced rather simply. If the rim members are all equal in length and approximate a circle when deployed, the angle between the axes of adjacent elements is $2\pi/N$ where N is the number of rim elements. The angles between the hinge axis and the axis of adjacent elements must be equal to each other so that the parallel packaged condition is possible.

Let us designate the orientation of the hinge axis by α and β, where α is the colatitude and β is the longitude of the hinge axis. We assume the deployed ring to be equatorial and measure β for each element from the direction of its right-hand end. Then the aforementioned equality of angles requires

$$\left.\begin{aligned} \beta &= \frac{\pi}{2} - \frac{\pi}{N} \text{ at the right-hand hinge} \\ &= \frac{\pi}{2} + \frac{\pi}{N} \text{ at the left-hand hinge} \end{aligned}\right\} \qquad \text{(A-1)}$$

We want to consider a deployment motion that is as symmetric as possible. Thus we require that every second hinge axis should describe exactly the same motion with respect to its deployed meridian. It can be shown that if one alternate set of hinge axes is constrained to follow the individual deployed meridians, then the other set of hinges also does so. Since the constraint only involves a rigid-body motion of the assembly, it can be imposed without loss of generality.

The symmetry assumption allows the complete specification of the state of the assembly in terms of the state of a single rim element. Such an element is shown in Figure A-1, together with the coordinate systems. The (X, Y, Z) system is inertially fixed; the (x, y, z) system is fixed to the element. Eularian angles ψ , θ , and φ specify the orientation of the lower-case system with respect to the upper-case system. The angle ψ is the rotation around the resulting y-axis; the angle φ is the rotation around the resulting (and final) x-axis. (These angles are the same as those of pitch, roll, and yaw in aircraft terminology.) The transformations from (x, y, z) to (X, Y, Z) are:

$$\begin{vmatrix} X \\ Y \\ Z \end{vmatrix} = \begin{bmatrix} \cos\psi\cos\theta & (-\sin\psi\cos\theta + \cos\psi\sin\theta\sin\varphi) & (\sin\psi\sin\varphi + \cos\psi\sin\theta\cos\varphi) \\ \sin\psi\cos\theta & (\cos\psi\cos\varphi + \sin\psi\sin\theta\sin\varphi) & (-\cos\psi\sin\varphi + \sin\psi\sin\theta\cos\varphi) \\ -\sin\theta & \cos\theta\sin\varphi & \cos\theta\cos\varphi \end{bmatrix} \begin{vmatrix} x \\ y \\ z \end{vmatrix} \quad \text{(A-2)}$$

The radius R to the center of the bar is related to the bar length ℓ and the angles θ and ψ by

$$(R - R_0) = \frac{\ell}{2}\cos\theta\,\frac{\cos\left(\psi - \frac{\pi}{N}\right)}{\sin\frac{\pi}{N}} \quad \text{(A-3)}$$

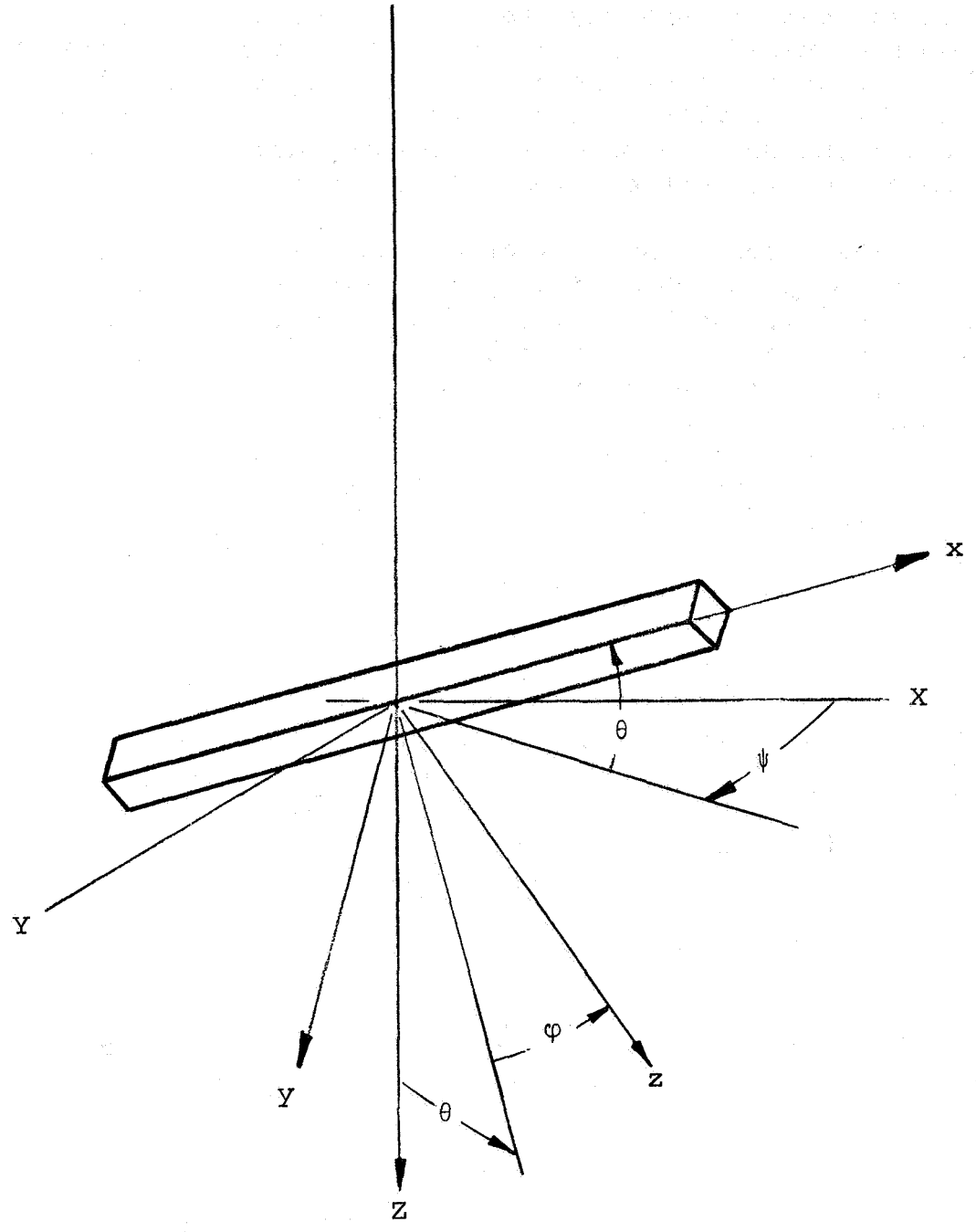

Figure A-1. Rim Element and Coordinate System

Let α_1 be the colatitude of the right-hand hinge. The direction cosines of this hinge axis are then ($\sin\alpha_1 \sin\delta$ $\sin\alpha_1 \cos\delta$, $\cos\alpha_1$) with respect to the body axes, where $\delta = \pi/N$. With respect to fixed axes they are

$$\left.\begin{aligned}
\ell_X &= (\sin\delta \cos\psi \cos\theta - \cos\delta \sin\psi \cos\varphi \\
&\quad + \cos\delta \cos\psi \sin\theta \sin\varphi) \sin\alpha_1 \\
&\quad + (\sin\psi \sin\varphi + \cos\psi \sin\theta \cos\varphi) \cos\alpha_1 \\
\ell_Y &= (\sin\delta \sin\psi \cos\theta + \cos\delta \cos\psi \cos\varphi \\
&\quad + \cos\delta \sin\psi \sin\theta \sin\varphi) \sin\alpha_1 \\
&\quad + (- \cos\psi \sin\varphi + \sin\psi \sin\theta \cos\varphi) \cos\alpha_1 \\
\ell_Z &= (- \sin\delta \sin\theta + \cos\delta \cos\theta \sin\varphi) \sin\alpha_1 \\
&\quad + \cos\theta \cos\varphi \cos\alpha_1
\end{aligned}\right\} \quad \text{(A-4)}$$

For the hinge on the left-hand end, the same process yields

$$\left.\begin{aligned}
\ell_X &= (- \sin\delta \cos\psi \cos\theta - \cos\delta \sin\psi \cos\varphi \\
&\quad + \cos\delta \cos\psi \sin\theta \sin\varphi) \sin\alpha_2 \\
&\quad + (\sin\psi \sin\varphi + \cos\psi \sin\theta \cos\varphi) \cos\alpha_2 \\
\ell_Y &= (- \sin\delta \sin\psi \cos\theta + \cos\delta \cos\psi \cos\varphi \\
&\quad + \cos\delta \sin\psi \sin\theta \sin\varphi) \sin\alpha_2 \\
&\quad + (- \cos\psi \sin\varphi + \sin\psi \sin\theta \cos\varphi) \cos\alpha_2 \\
\ell_z &= (\sin\delta \sin\theta + \cos\delta \cos\theta \sin\varphi) \sin\alpha_2 \\
&\quad + \cos\theta \cos\varphi \cos\alpha_2
\end{aligned}\right\} \quad \text{(A-5)}$$

where α_2 is the colatitude of the left-hand hinge axis.

As pointed out previously, we require that the right-hand hinge axis remain on the same meridian. This requires

$$\ell_X \cos\delta = \ell_Y \sin\delta$$

The result is

$$\begin{aligned} 0 = {} & (\sin\delta \cos\delta \cos\psi \cos\theta - \sin^2\delta \sin\psi \cos\theta - \cos^2\delta \sin\psi \cos\varphi \\ & - \sin\delta \cos\delta \cos\psi \cos\varphi + \cos^2\delta \cos\psi \sin\theta \sin\varphi \\ & - \sin\delta \cos\delta \sin\psi \sin\theta \sin\varphi) \sin\alpha_1 + (\cos\delta \sin\psi \sin\varphi \\ & + \sin\delta \cos\psi \sin\varphi + \cos\delta \cos\psi \sin\theta \cos\varphi \\ & - \sin\delta \sin\psi \sin\theta \cos\varphi) \cos\alpha_1 \end{aligned} \qquad \text{(A-6)}$$

For the left-hand hinge, the result is the same except that δ is replaced by $-\delta$ and α_1 by α_2.

If we pick values for α_1 and α_2, then the two equations can be satisfied by properly selecting ψ and φ for each θ between 0 and $\pi/2$. This process, however, may not yield results for some ranges of θ due to the limits on the trigonometric functions. If α_1 and α_2 are selected as $\pi/2$, for instance, examination shows that $\sin^2\theta$ must be less than $1/4 \cos^2\delta$.

In order to investigate further, let us consider the case where $\alpha_2 = \pi - \alpha_1$. Then the terms in the left-hand and right-hand equations are the same except for sign.

Collecting same-sign and opposite-sign terms gives

$$\begin{aligned} & (-\sin^2\delta \sin\psi \cos\theta - \cos^2\delta \sin\psi \cos\varphi \\ & + \cos^2\delta \cos\psi \sin\theta \sin\varphi) \sin\alpha_1 \\ & + (\cos\psi \sin\varphi - \sin\psi \sin\theta \cos\varphi) \sin\delta \cos\alpha_1 = 0 \end{aligned} \qquad \text{(A-7)}$$

and

$$(\cos\psi\cos\theta - \cos\psi\cos\varphi - \sin\psi\sin\theta\sin\varphi)\sin\delta\sin\alpha_1 + (\sin\psi\sin\varphi + \cos\psi\sin\theta\cos\varphi)\cos\alpha_1 = 0 \quad \text{(A-8)}$$

The determinant of the coefficients of $\sin\psi$ and $\cos\psi$ must be zero for a solution to be possible. Thus

$$\begin{vmatrix} (-\sin^2\delta\cos\theta - \cos^2\delta\cos\varphi)\sin\alpha_1 & \cos^2\delta\sin\theta\sin\varphi\sin\alpha_1 \\ -\sin\delta\sin\theta\cos\varphi\cos\alpha_1 & +\sin\delta\sin\varphi\cos\alpha_1 \\ -\sin\delta\sin\theta\sin\varphi\sin\alpha_1 & \sin\delta(\cos\theta - \cos\varphi)\sin\alpha_1 \\ +\sin\varphi\cos\alpha_1 & +\sin\theta\cos\varphi\cos\alpha_1 \end{vmatrix} = 0 \quad \text{(A-9)}$$

If we set $\theta = \frac{\pi}{2}$, we get

$$\begin{vmatrix} -(\cos^2\delta\sin\alpha_1 & (\cos^2\delta\sin\alpha_1 \\ +\sin\delta\cos\alpha_1)\cos\varphi & +\sin\delta\cos\alpha_1)\sin\varphi \\ (\cos\alpha_1 - \sin\delta\sin\alpha_1)\sin\varphi & (\cos\alpha_1 - \sin\delta\sin\alpha_1)\cos\varphi \end{vmatrix} = 0 \quad \text{(A-10)}$$

Expanding gives

$$(\cos^2\delta\sin\alpha_1 + \sin\delta\cos\alpha_1)(\cos\alpha_1 - \sin\delta\sin\alpha_1) = 0 \quad \text{(A-11)}$$

Thus, a candidate design hinge axis would have

$$\cos\alpha_1 = -\frac{\cos^2\delta}{\sin\delta}\sin\alpha_1 \quad \text{(A-12)}$$

The other possibility leads to complicated motions.

In order to assure the validity of such a hinge axis angle, we must determine the manner in which the various coordinates change during transition between $\theta = 0$ and $\pi/2$.

Using Equation (A-12) in Equation (A-9) and expanding yields

$$\cos^2\delta \cos^2\theta \cos^2\varphi - \sin^2\delta [\cos^2\delta (1+\sin\theta) - \sin\theta] \cos\theta \cos\varphi - (1-\sin\theta)(1-2\sin^2\delta \cos^2\delta + \sin^2\delta \sin\theta) = 0 \quad \text{(A-13)}$$

The solution of this quadratic equation yields two values for $\cos\varphi$. We pick the branch for which $\cos\varphi = 1$ for $\theta = 0$. This branch, of course, yields two values for φ (positive and negative). Both results have meaning.

Substituting Equation (A-12) into Equation (A-7) allows the determination of ψ. Thus

$$\tan\psi = -\frac{\sin\varphi}{\cos\varphi + \tan^2\delta \frac{\cos\theta}{1-\sin\theta}} \quad \text{(A-14)}$$

Choice of positive or negative values for φ produces negative or positive values for ψ.

Results are shown in Figures A-2(a), (b), (c), and (d) for N = 4, 6, 10, and 90, respectively. In these figures the values of φ and the corresponding values of ψ are plotted versus θ.

Note that real results are obtained in all cases for the complete range of θ from 0° to 90°. Note that, on the other hand, negative values of θ are not included. Indeed, an implicit assumption of positive θ was introduced in the development leading to Equation (A-12). Examination shows that the sign of θ must be opposite to the sign of $\cos\alpha_1$ (see Eq. (A-9)). The assumption $\alpha_2 = \pi - \alpha_1$ implies that $\cos\alpha_1$ retains its magnitude but switches sign from member to member around the rim. So, therefore, does θ. Examination of Equations (A-7) and (A-8) shows that holding the sign of φ constant but switching the signs of θ, ψ, and $\cos\alpha_1$ leaves

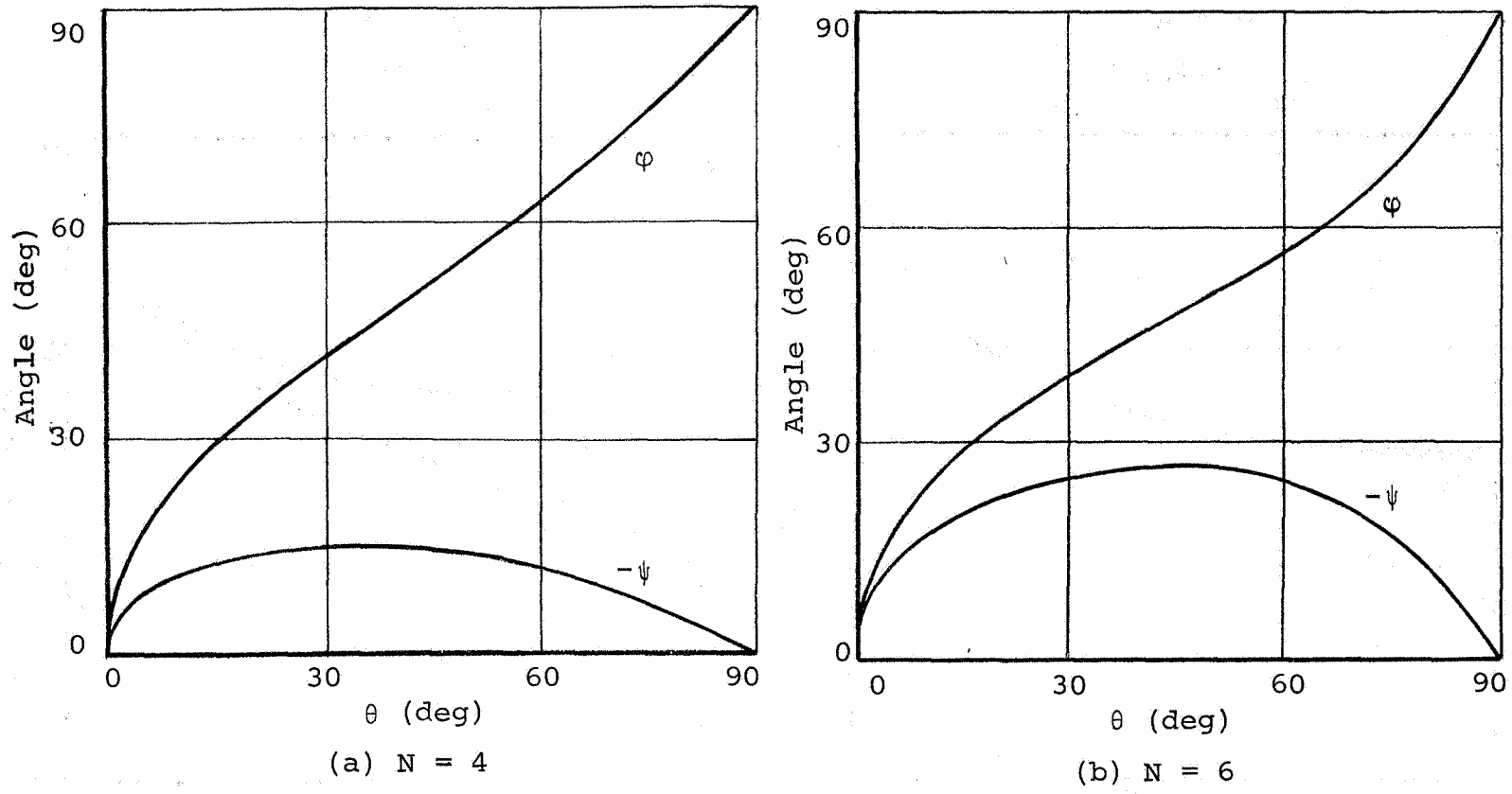

Figure A-2. Variation of Eulerian Angles During Stowage

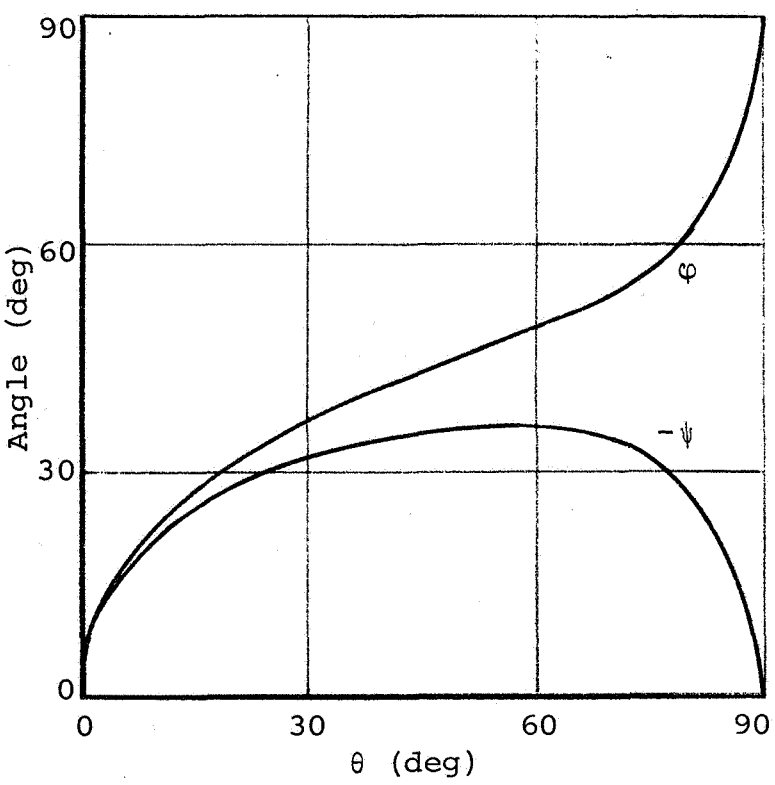

(c) N = 10

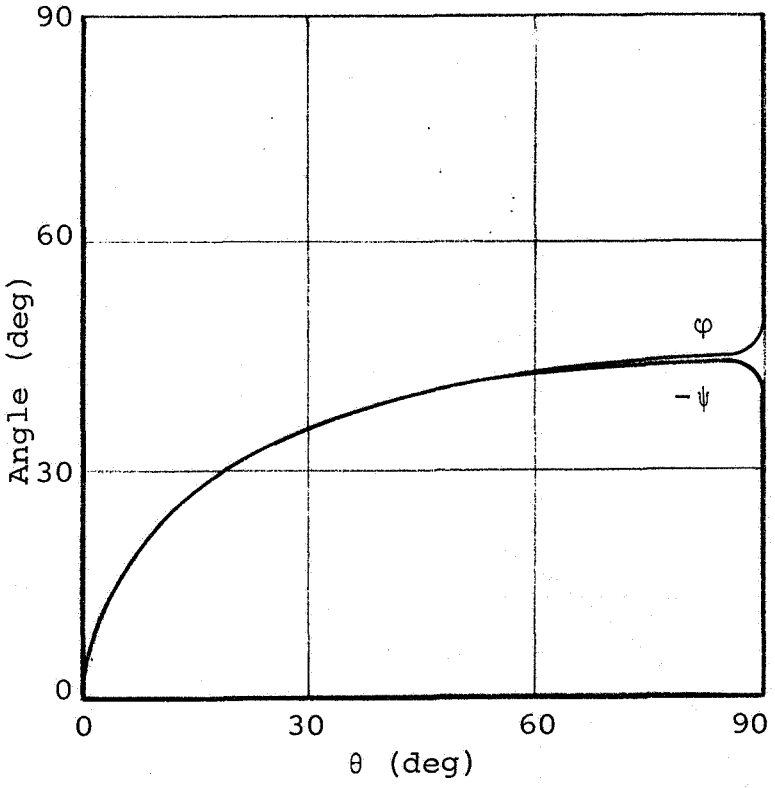

(d) N = 90

Figure A-2 (Continued)

the equations unchanged. Therefore, all kinematic conditions are satisfied and the deployment is feasible.

Characteristics of Deployment

The manner in which the deployment proceeds can be deduced from Figure A-2. For large values of N (see Fig. A-2(d)), the elements exhibit large variations of roll (φ) and yaw (ψ) for very small changes in pitch (θ). The planform of the partially deployed ring thus looks like an N/2 pointed star with right-angle points. As the pitch angle θ decreases, the "star" grows in size and its point angles become more obtuse. Finally, the elements all become level in the final N-sided regular polygon.

These characteristics can be seen in Figure A-3. A ten-sided model was constructed and photographed in various stages of deployment. The stellate nature of the deployment is apparent.

The proper location of the hinge axis can be accomplished in a rather straightforward fashion. The mating ends of the elements are geometrically like an upward pointing truncated wedge with inner and outer sides at an angle $\delta(= \pi/N)$ to the vertical. These mating ends are then faced off to produce the proper miter. Hinges are then mounted alternately on the inside and outside sloping sides. The wooden model shown in Figure A-3 was constructed with uniform-wedge elements. In full-scale hardware, of course, only the ends need to be so treated. The remainder of the element needs to be shaped in such a fashion only to permit appropriate nesting for stowage.

The stellate character of deployment may present problems with respect to interfacing with other portions of the system. For this reason, other possible hinge arrangements were partially investigated. Although a complete study was not made, it appears that alternative orientations would produce even more complicated motions. Apparently, therefore, the hinge geometry studied herein is the simplest possible way of constructing a deployable multisided rim.

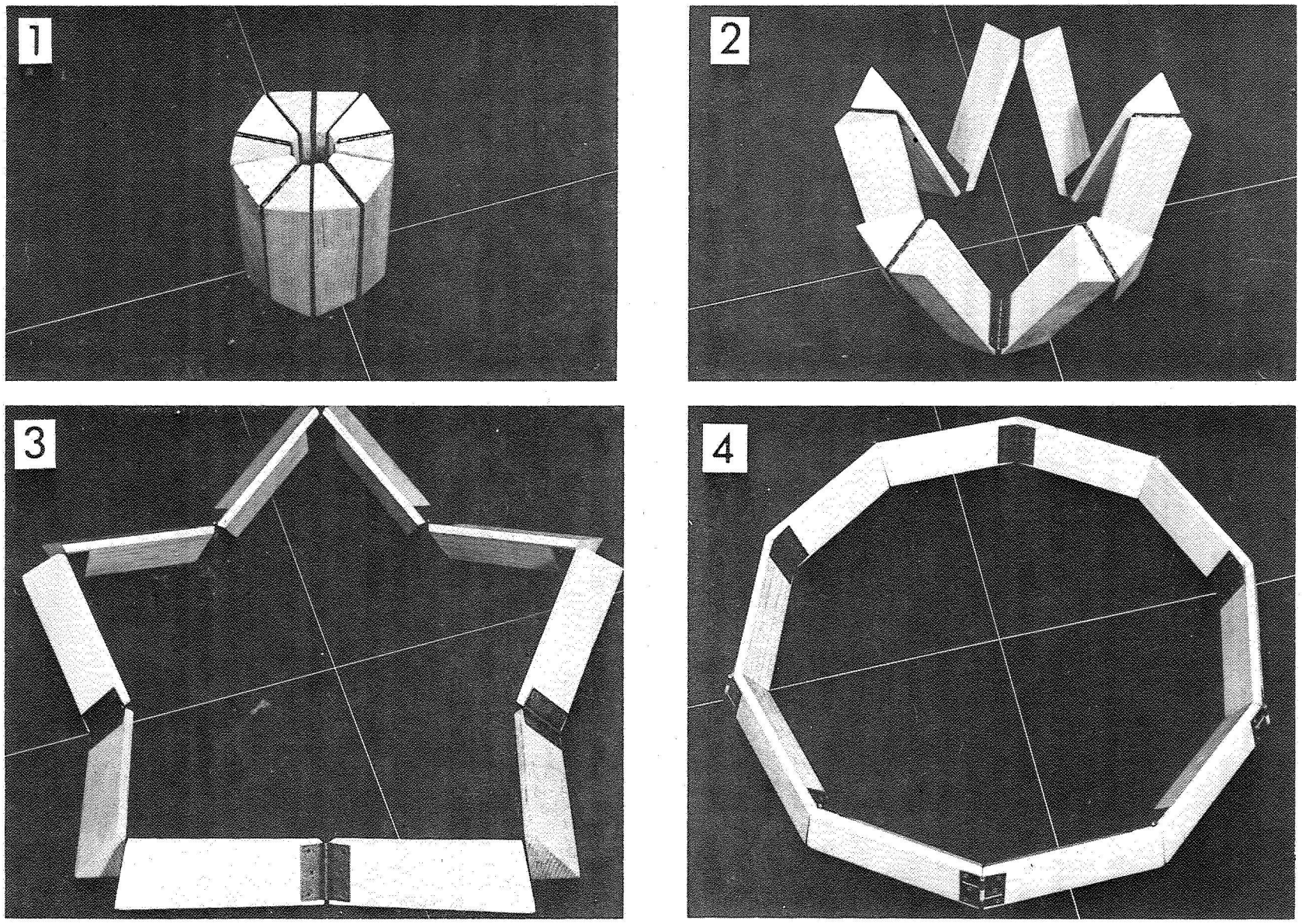

Figure A-3. Deployment of Ten-sided Model Rim

APPENDIX B

SCALING LAWS FOR SOLAR ARRAYS

The vibrational frequency of a rectangular solar-cell blanket is directly proportional to its tension and inversely proportional to the square of its length; hence:

$$f \alpha \frac{T}{L^2}$$

When the array is unidirectionally tensioned between two bars, and when the bars are kept separated by an efficiently designed tubular boom, Euler-buckling considerations will govern the boom design. Therefore,

$$T \alpha \frac{I}{L^2}$$

where I is the section moment of inertia for the boom. For a furlable, tubular boom, the thickness-to-diameter ratio of the boom will be approximately constant (see Ref. 11). Therefore,

$$I \alpha d^4$$

where d = boom diameter

The boom weight W_B is proportional to d^2L, so that

$$I \alpha \frac{W_B^2}{L^2}$$

The weight of all the components comprising the structure of a boom-deployed solar array is estimated to be directly proportional to the weight of its boom. Therefore,

$$W_S \alpha W_B$$

This leads to $$f^2 \alpha \frac{W_S^2}{L^6}$$

However, the blanket area is proportional to L^2. Accordingly,

$$W_S \alpha fA^{3/2}$$

The structural weight fraction G can then be scaled as follows:

$$G = \frac{1}{1 + \frac{K}{fA^{1/2}}}$$

where K is a constant that can be evaluated from the properties of a known solar-array system. This scaling law may be used if the frequency is to remain the same for the scaled system.

However, assume that the primary reason for specifying the necessary vibrational frequency for a solar array is to ensure that the array does not resonate with, or otherwise adversely interact with, the control system. Further, assume that the primary function of the control system is to keep the solar array sun-oriented within a prescribed angular accuracy β. Control torques τ applied to such a system are:

$$\tau = mA\rho^2\ddot{\beta}$$

where ρ = radius of gyration of the system

But assume $$\rho \alpha A^{1/2}$$

Also assume that the control impulses are cyclic; then

$$\ddot{\beta} \alpha f_c^2 \beta$$

where f_c = frequency of impulses

Then $$\tau \alpha mA^2 f_c^2 \beta$$

Assume that the control torques must counteract and be directly proportional to the perturbing torques on the system.

Finally, assume that the latter are proportional to the mass of the system times a characteristic dimension of it. This leads to:

$$\tau \quad \alpha \quad mA \times A^{1/2}$$

This proportionality may apply, for example, to gravity-gradient torques, or to solar pressure acting eccentrically:

$$\tau \quad \alpha \quad A^{3/2}$$

For a scaling law that applies to either type of perturbing torque, the mass density of the blanket is omitted from consideration. Also note that the blanket density can be expected to be a constant, i.e., a function of the state of technology and not of the scale. Then:

$$f_c^{\,2} \quad \alpha \quad \frac{1}{\beta A^{1/2}}$$

A reasonable criterion for the vibrational frequency of the system is:

$$\frac{f}{f_c} = \text{constant}$$

Also, β may be prescribed independent of A. Accordingly,

$$f \quad \alpha \quad A^{-1/4}$$

The structural weight fraction for the boom-deployed type of solar-array system can then be scaled as follows:

$$G = \frac{1}{1 + KA^{-1/4}}$$

where size-independent values of m and β are prescribed.

REFERENCES

1. Wolff, George; and Wittmann, Alois: The Flight of FRUSA. AIAA Paper No. 72-510, AIAA Ninth Electric Propulsion Conference (Bethesda, Maryland), April 1972.

2. Hasbach, W. A.: Design and Development of a 66-W/kg, 23-m^2 Roll-Up Solar Array. JPL Quarterly Technical Review, Vol. I, No. 1, April 1971, pp. 68-77.

3. Anon.: Design and Analysis - Space Station Solar Array Technology Evaluation Program. LMSC-A995719, Lockheed Missiles and Space Company, November 1971.

4. Coyner, J. V., Jr. and Ross, R. G.: Parametric Study of the Performance Characteristics and Weight Variations of Large-Area Roll-Up Solar Arrays. NASA Technical Report 32-1502, December 1970.

5. Pope, D. L.; and Hewitt, W. H., Jr.: Construction and Evaluation of a Lightweight Parabolic Antenna Model. AIAA Paper No. 71-397, ASS/AIAA Variable Geometry and Expandable Structures Conference (Anaheim, California), April 1971.

6. Oliver, R. E.: Large Spacecraft Antennas: New Geometric Configuration Design Concepts. JPL Quarterly Technical Review, Vol. I, No. 1, April 1971, pp. 78-85.

7. Ruze, J.: Antenna Tolerance Theory - A Review. Proc. IEEE, Vol. LIV, No. 4, April 1966, pp. 633-640.

8. Anon.: Buckling of Thin-Walled Circular Cylinders. NASA Space Vehicle Design Criteria (Structures), NASA SP-8019, revised 1968.

9. Timoshenko, S.: Theory of Elastic Stability. McGraw-Hill Book Company Inc., New York, 1936, p. 108.

10. Shanley, F. R.: Weight-Strength Analysis of Aircraft Structures. McGraw-Hill Book Company Inc., New York, 1952, pp. 15-22.

11. Crawford, R. F.: Strength and Efficiency of Deployable Booms for Space Applications. AIAA Paper No. 71-396, AAS/AIAA Variable Geometry and Expandable Structures Conference (Anaheim, California), April 1971.

12. MacNeal, Richard H.; Hedgepeth, John M.; and Schuerch, Hans U.: Heliogyro Solar Sailer Summary Report. NASA CR-1329, June 1969.

NATIONAL AERONAUTICS AND SPACE ADMINISTRATION
WASHINGTON, D.C. 20546

OFFICIAL BUSINESS
PENALTY FOR PRIVATE USE $300

SPECIAL FOURTH-CLASS RATE BOOK

POSTAGE AND FEES PAID
NATIONAL AERONAUTICS AND SPACE ADMINISTRATION
451

U.S. MAIL

POSTMASTER: If Undeliverable (Section 158 Postal Manual) Do Not Return

"The aeronautical and space activities of the United States shall be conducted so as to contribute . . . to the expansion of human knowledge of phenomena in the atmosphere and space. The Administration shall provide for the widest practicable and appropriate dissemination of information concerning its activities and the results thereof."

—NATIONAL AERONAUTICS AND SPACE ACT OF 1958

NASA SCIENTIFIC AND TECHNICAL PUBLICATIONS

TECHNICAL REPORTS: Scientific and technical information considered important, complete, and a lasting contribution to existing knowledge.

TECHNICAL NOTES: Information less broad in scope but nevertheless of importance as a contribution to existing knowledge.

TECHNICAL MEMORANDUMS: Information receiving limited distribution because of preliminary data, security classification, or other reasons. Also includes conference proceedings with either limited or unlimited distribution.

CONTRACTOR REPORTS: Scientific and technical information generated under a NASA contract or grant and considered an important contribution to existing knowledge.

TECHNICAL TRANSLATIONS: Information published in a foreign language considered to merit NASA distribution in English.

SPECIAL PUBLICATIONS: Information derived from or of value to NASA activities. Publications include final reports of major projects, monographs, data compilations, handbooks, sourcebooks, and special bibliographies.

TECHNOLOGY UTILIZATION PUBLICATIONS: Information on technology used by NASA that may be of particular interest in commercial and other non-aerospace applications. Publications include Tech Briefs, Technology Utilization Reports and Technology Surveys.

Details on the availability of these publications may be obtained from:

SCIENTIFIC AND TECHNICAL INFORMATION OFFICE

NATIONAL AERONAUTICS AND SPACE ADMINISTRATION

Washington, D.C. 20546